Applied Energy 358 (2024) 122564

Contents lists available at ScienceDirect

Applied Energy

journal homepage: www.elsevier.com/locate/apenergy

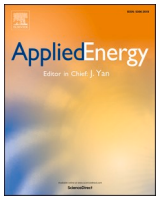

Reduced desalination carbon footprint on islands with weak electricity grids. The case of Gran Canaria

Pedro Cabrera [a,*], José A. Carta [a], Carlos Matos [a], Enrique Rosales-Asensio [b], Henrik Lund [c]

[a] Department of Mechanical Engineering, University of Las Palmas de Gran Canaria, Campus de Tafira s/n, 35017 Las Palmas de Gran Canaria, Canary Islands, Spain
[b] Department of Electrical Engineering, University of Las Palmas de Gran Canaria, Campus de Tafira s/n, 35017 Las Palmas de Gran Canaria, Canary Islands, Spain
[c] Department of Sustainability and Planning, Aalborg University, Rendsburggade 14, Denmark

HIGHLIGHTS

- A method for achieving large-scale, low-carbon desalination is presented.
- Optimal wind farm and storage capacities for the system are determined.
- The method offers substantial CO2 emission reduction potential.
- Using climate ERA5 reanalysis data, enhances robustness by addressing wind variability.
- Proposed adjustments enhance adaptability to technological advances and future scenarios.

GRAPHICAL ABSTRACT

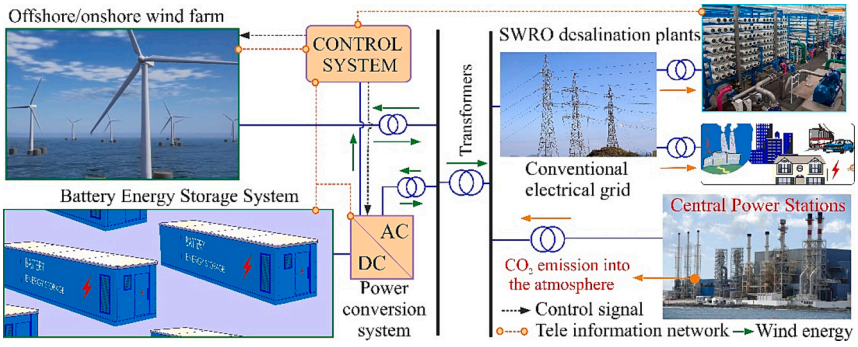

ARTICLE INFO

Keywords:
On-grid wind desalination
Off-grid wind desalination
Zero-carbon footprint
Reverse osmosis
Desalination
Energy
Renewable energy
Smart energy system

ABSTRACT

The aim of this paper is to present options to make low-carbon footprint large-scale desalination a reality on arid islands with weak electrical grids. Through these options, the goal is to reconfigure on-grid wind energy/desalination systems for large- and medium-scale water production. In this context, it is proposed to use lithium-ion batteries for stationary energy storage together with management strategies aimed at avoiding the wind energy/desalination systems having to consume energy from the conventional grid they are connected to. The control strategy is based on ensuring that the power provided by the wind farm and batteries remains in synchrony with the power demand of the desalination plant throughout the system's useful life. The interannual variation of wind energy is considered when sizing the renewable energy system and processes for its estimation are proposed. The case study is centred on the Canary Archipelago, a region that is especially vulnerable to the impacts of climate change, but which enjoys exceptional characteristics for the exploitation of wind energy. The results obtained show the optimal wind farm and energy storage system capacities of the analysed configurations. The approach presented allows a low-carbon operational footprint. If the control strategy were to be put into practice today, the current grid restrictions and a life cycle assessment of the system carried out in a societal context that continues to be fossil fuel dependent indicate a potential reduction of 77.4% of the footprint. However, the remaining 22.6% could be eliminated in the future when the manufacturing processes of wind turbines, batteries and desalination plants receive the benefits of carbon-neutral societies.

* Corresponding author.
E-mail address: pedro.cabrerasantana@ulpgc.es (P. Cabrera).

https://doi.org/10.1016/j.apenergy.2023.122564
Received 15 September 2023; Received in revised form 18 November 2023; Accepted 25 December 2023
Available online 13 January 2024

1. Introduction

According to the United Nations World Water Development Report 2020 [1], use of water worldwide has increased sixfold over the last 100 years and continues to rise at a constant annual rate of 1%. This rise is associated to greater agricultural and industrial use, population and economic growth, changing consumer patterns and the effects of climate change [2]. The latter of these causes reduces the predictability of the availability of water and aggravates the situation in regions where water scarcity is greatest.

In the last four decades, the increase in water consumption has led to a rise in the construction of desalination plants as part of the attempt to mitigate the scarcity of this resource [3]. This is taking place in numerous islands in the European Union (EU) [4], including those in the Canary Archipelago [5], as well as in other parts of the world [6].

One of the problematic issues in the employment of desalination processes is their intensive energy consumption, although the industry has already made important strides in its reduction [7]. The prevailing trend is towards the implementation of SWRO plants driven by electrical energy [8].

Traditionally, the energy sources used in water desalination processes have been of fossil fuel origin [9]. According to [10], the

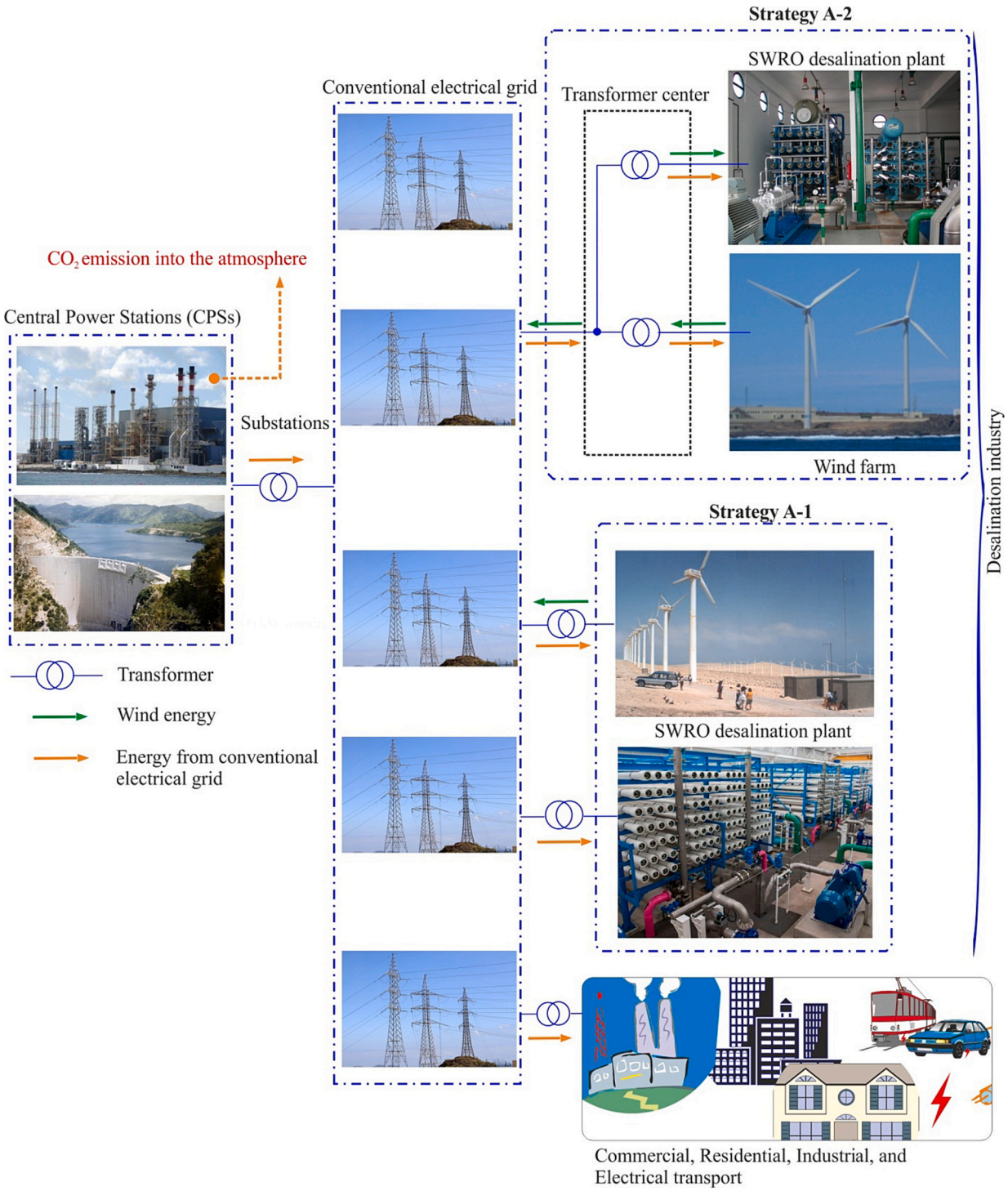

Fig. 1. On-grid wind energy systems for water desalination.

desalination plants currently in operation in the world emit around 76 million tonnes of CO_2 annually. In [11], with the caveat that more analyses are required to improve the precision of the estimation, the amount is calculated to be even higher, at 120 million tonnes per year. In [10], it is calculated that if low carbon options are not implemented the amount will rise to 218 million tonnes by 2040.

Given the importance of the water-energy binomial, one of the aims in the desalination industry must be the replacement of fossil fuels with other non-polluting renewable energy sources using mature and low-cost technologies [12,13].

1.1. Literature review on installed renewable energy desalination systems on islands

Currently, only around 1% of desalinated water comes from renewable energy-sourced desalination systems (RES-desalination systems) [14]. However, in several regions with water scarcity problems, different aspects related to the water-energy nexus have been tackled based on the implementation of RES-desalination systems. Given the high level of maturity of wind energy-associated technologies, this is one of the most commonly used renewable energy sources in large-scale desalination [11,15], especially in coastal areas with high wind potential [16].

According to Karimanzira [17], the electrical energy generated by wind technology costs less than other renewable energy sources. In another study, the same author [18] recommends this as the first option in combination with a reverse osmosis desalination system to produce freshwater using sustainable energy.

The RES-desalination systems that have been installed on islands can be classified in two major groups [8]: A) on-grid renewable energy technologies (Fig. 1); and B) off-grid renewable energy technologies (Fig. 2).

1.1.1. Literature review on installed on-grid renewable energy systems for water desalination

To date, the owners of large- and medium-scale desalination plants have opted for the use of on-grid renewable energy systems for water desalination or, in other words, for the installation of renewable energy technologies (principally wind) and the connection of the two subsystems to conventional power distribution grids [9]. Such projects basically use two strategies (referred to in this paper as A-1 and A-2) for renewable energy and conventional energy management when it comes to powering the desalination plants (Fig. 1). In the A-1 strategy, the renewable energy technology feeds all the energy that it generates into the conventional grid and the desalination plant is treated like another load in the system.

When used in weak energy systems in which a significant renewable power needs to be installed to meet a high freshwater demand, this strategy can generate problems of instability in the power system [9,19]. In this context, some authors have reported that the integration of renewable-powered desalination in the conventional grids of isolated islands may be limited even in the case of high renewable energy potential [20]. However, interesting methods based on the *Smart Energy Systems* concept [21,22] have been proposed to manage the optimal

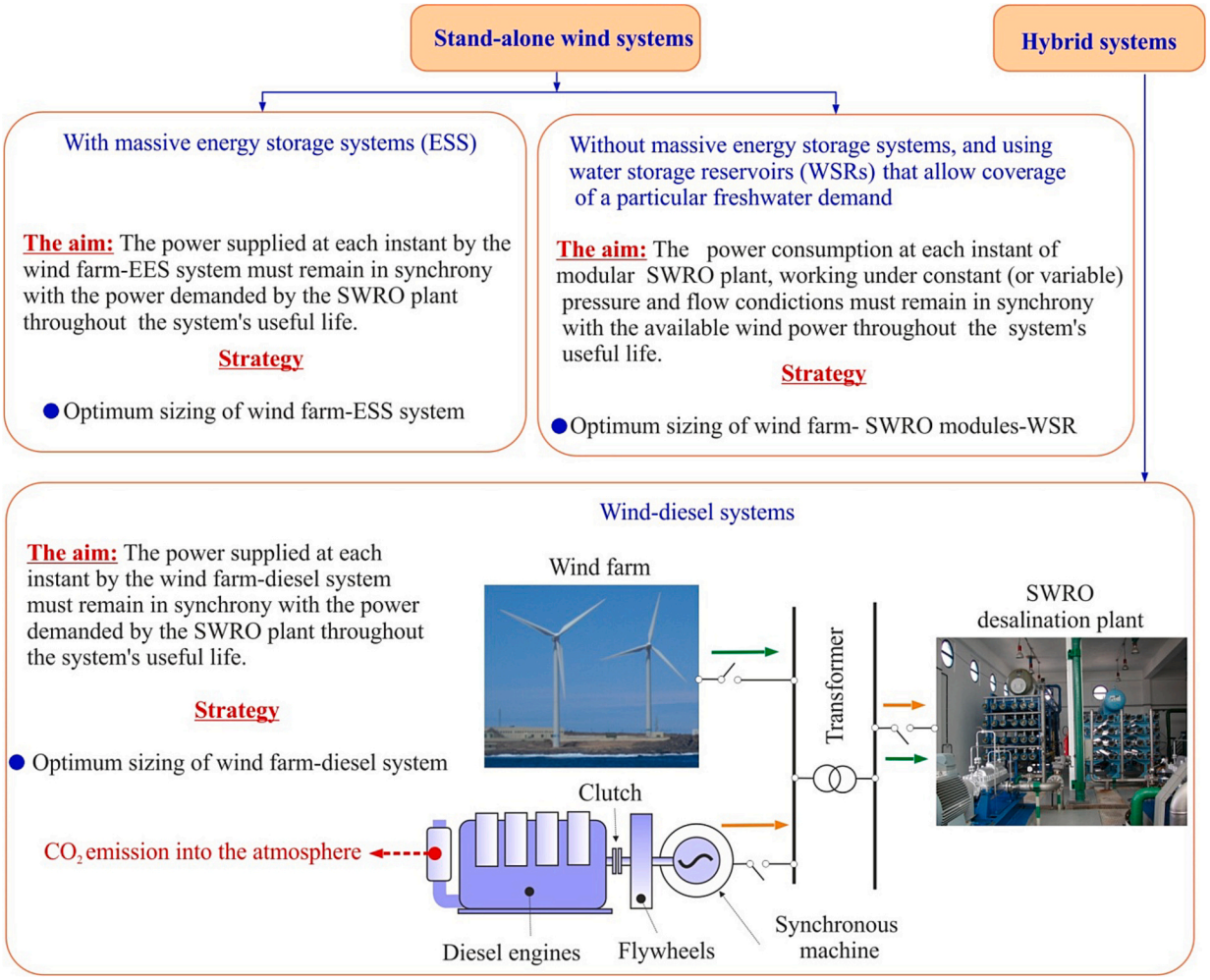

Fig. 2. Off-grid wind energy systems for water desalination.

large-scale integration of renewable power in water-energy systems on islands and increase the contribution of renewables to the primary energy supply of the islands [23]. Such methods consider the water desalination and treatment systems as flexible loads and explore a wide range of possible water supply infrastructures and renewable energy combinations (wind and solar). *Smart Energy Systems* represent a holistic strategy that harmonizes the integration of different sectors to unearth the potential synergies within, striving to attain the most efficient outcomes for every sector within the energy landscape. Unlike the more singular emphasis of the Smart Grid concept, which primarily centrs on electricity, this approach considers the entirety of the energy ecosystem [24], delving into the exploration of suitable infrastructure blueprints and operational approaches to enhance the energy system as a whole [25].

In the A-2 strategy the renewable energy technologies must be permanently connected to the desalination plants through a direct connection independent from the conventional grid [9]. As a result, the renewable technology needs to be installed in an area close to that of the desalination plant whose energy consumption it is associated to. In this strategy, the electrical energy generated by the renewable energy technology is used primarily to cover the instantaneous energy needs of the desalination plant (Fig. 1). In this case, the mismatches in instantaneous energy between the electrical energy generation of the renewable energy technology and the consumption of the desalination plant are corrected by taking from the conventional grid the amount of energy that is required and by feeding into the grid any surplus renewable energy production.

1.1.2. Literature review on installed off-grid renewable energy systems for water desalination

To date, in practically all cases, installations of off-grid renewable energy systems for water desalination are comprised of microgrids that have been configured to handle mostly very small-scale desalination, and generally using batteries as an energy storage system. In the case of using a renewable technology operating in parallel with diesel-operated generators (Fig. 2), a zero-carbon operational footprint is not possible. However, in other off-grid renewable energy systems that do not use diesel, a low-carbon water desalination footprint can be achieved if considering only the operating life of the system.. Larger-scale microgrids have also been deployed in which no massive energy storage systems are used (Fig. 2). Examples where such microgrids have been employed include the islands of Syros (Greece) [26], Rügen (Germany) [27], Borkum (Gemany) [27], Symi (Greece) [9,28], Tenerife (Canary Islands, Spain) [26] and Gran Canaria (Canary Islands, Spain) [29–31].

1.1.3. Literature review on proposed large-scale RE-desalination systems on arid islands

Different configurations and strategies have been proposed in the literature to cover the needs of islands. Segurado et al. [20] proposed the connection of a wind farm (WF) and SWRO plant (5400 m^3/d) to the conventional power distribution grid for the island of S. Vicente (Cape Verde). To mitigate the problems associated to the weakness of the electrical grid [19], the construction of a pumped hydro storage system was proposed. Mentis et al. [32] proposed optimal RES-desalination configurations for three islands in the South Aegean Sea, Patmos (2000 m^3/d), Lipsoi (400 m^3/d) and Thirasia (100 m^3/d), with the desalination system connected to the grid and powered using RES and fossil fuels only when necessary. Configurations have also been proposed that aim to cover only a percentage of the water demand of an island.

Proposals for off-grid RES-desalination systems include the one presented for an area in Gran Canaria [33] which considered the installation of a microgrid comprising a modular SWRO desalination plant (8 modules of 1000 m^3/d capacity: 8000 m^3/d) -powered exclusively by off-grid wind energy- and a water storage reservoir (65,900 m^3) to allow coverage of a freshwater demand of 1825 $\times$ 10^3 m^3/year without the use of massive energy storage devices. The system they proposed was configured based on the experience acquired with a microgrid that had previously been installed and tested on the same island [29]. This microgrid, which forms part of a wider programme titled the Sea Desalination Autonomous Wind Energy System (SDAWES) [30,31], takes advantage of the modular nature of SWRO plants, connecting and disconnecting modules which operate under constant pressure and flow conditions. The configuration of the microgrid and its operating strategy permit its extrapolation to large-scale wind-powered water production without a back-up energy provider [29]. In the proposal that they presented in [33], the authors took advantage of the experience acquired with a wind turbine-powered prototype SWRO plant designed and tested to operate under variable flow and feed pressure conditions [34,35].

1.2. Aim, novelty and key contributions of this paper

The aim of this paper is to present options to make low-carbon footprint large-scale desalination a reality on arid islands with weak grids. The key contribution of this paper is the proposal to reconfigure wind energy systems that operate with the A-1 strategy (Fig. 1) so that they do not need to consume energy from the conventional grid they are connected to or diesel generators that are generally proposed [36,37] as an auxiliary power source when supplying energy to the WF and ancillary services in island-based operation. In this study, the use is proposed of grid-forming (GFM) converters, comprised of battery energy storage systems (BESSs), to guarantee service availability. More specifically, to avoid the use of fossil fuels the implementation is proposed of lithium-ion batteries (LIBs) for medium- and large-scale stationary energy storage together with specific system management strategies. According to Pagnani et al. [38], given their scalability, response time and capacity to absorb and deliver energy to the system, BESSs are a good option to smooth wind energy generation and increase the stability of energy systems. In this work, the objective is for the wind-sourced electrical power to be in synchrony at each instant with the power demand of the SWRO plants, taking into consideration the energy losses generated in the transport of this power from the generation points to the consumption points. In the configurations considered in this paper, as well as balancing mismatches between SWRO plant power demand and WF-generated power, the purpose of the LIBs, as is proposed in the literature, is to ensure service availability. In other words, the goal is that power can be supplied to the central control of the system and ensure that the power required by the different devices (yaw mechanism, blade-pitch control, etc.) of the wind turbines (WTs) and by the ancillary components of the proposed on-grid system is covered in periods in which insufficient wind energy is available. In addition, the proposed method considers the interannual variation of wind energy and the use of procedures based on climate reanalysis data [39] if no historical meteorological data are available of the study site. This approach differs substantially from the standard approaches which use a time series that covers just a single year.

It should be noted that the A-1 strategy has the advantage over the A-2 strategy that selection of the WF site can be selected on the basis of the relevance of its energy resource and that of the SWRO plant coastal site on the basis of optimal technical, economic and environmental impact characteristics [40]. The tasks of the proposed algorithm for the optimal sizing of the electrical energy generation system and the simulation of large-scale wind-powered SWRO plants include selecting the optimal number of WTs and determining the capacities of the LIBs required for the proper functioning of the system such that SWRO plant energy demand is covered at each instant. This island has an energy policy that promotes the use of RES-desalination systems and enjoys exceptional potential for the exploitation of wind energy [41].

2. Method

In this section, a description is first provided of the general configuration of the systems proposed as options to make low-carbon footprint large-scale desalination a reality on arid islands with weak grids. The tasks of the algorithm of the method for the optimal sizing and simulation of large-scale wind powered SWRO plants are then described.

2.1. Description of the general reconfiguration of the on-grid system with strategy A-1

Fig. 3 provides a rough schematic outline of the general configuration of the proposed system. The on-grid renewable electrical generation system can be seen on the left, with the central power stations (CPSs) below.

On the right-hand side of Fig. 3 is the conventional electrical grid to which the SWRO desalination plants are connected in a similar manner to the commercial, residential, industrial and electrical transport customers of the island.

The WF will comprise one or more WTs and, given the consideration of island-based implementation, may be onshore or offshore. It should be noted that in the latter case, although not included in the rough schematic outline of the general configuration of the proposed system of Fig. 3, there are various alternatives for offshore-to-onshore energy transport [19], none of which have implications for the method proposed in this paper. A BESS, with a bidirectional power conversion subsystem (PCS), also forms part of the electrical generation subsystem. The purpose of the BESS is to balance the mismatches between SWRO plant power demand and WF-generated power. In addition, the BESS has to supply energy to the control subsystem (CS), the WT devices (yaw mechanism, blade-pitch control, etc. [42]) when required, and the ancillary components of the system, including step-up substations [36,37,43,44], reactive energy compensators, power electronic converters, etc. In the scenario of the use of offshore WFs, given the potentially large size of the GFM BESS and the consequent complications for its installation, as highlighted by Pagnani et al. [45], its onshore installation is proposed.

The CS acquires, through a tele information network (Fig. 3), data on SWRO plant energy consumption to facilitate management of the wind-sourced electrical energy that the renewable generation system needs to inject into the conventional grid art each instant. The CS also receives data on the operating parameters of the WF and the BESS and is responsible for supervision of the entire energy system operating process. The renewable generation system is coupled to a conventional electrical grid substation.

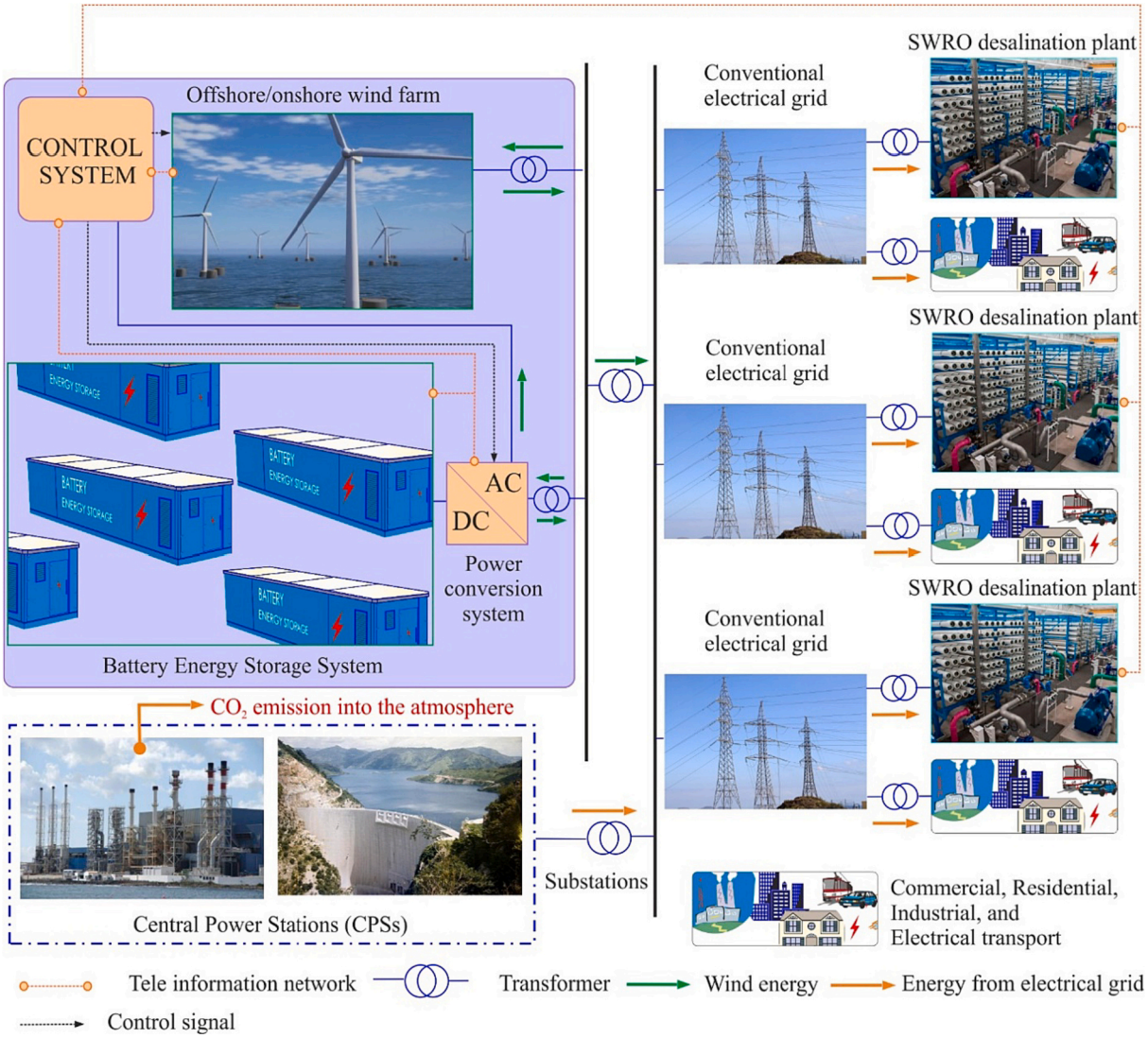

Fig. 3. Proposed on-grid option to make low-carbon footprint large-scale desalination a reality on arid islands with weak grids.

2.2. Overall description of the method

Fig. 4 shows a schematic representation of the method applied in this research, referring to the different sections, equations and figures where the set of tasks proposed are described in detail. The method selects the economically optimal system comprising a stand-alone WF, consisting of a particular number of WTs, *NWT*, and a BESS that allows coverage of a particular hourly freshwater demand.

The first task in the proposed method is to estimate the long-term wind resource at the target site. It is assumed that there are no historical data series available and that only a short series of data is available for the target site or its surroundings. It is proposed to use ERA5 climate reanalysis, data [39]. ERA5 is a global climate reanalysis product from the European Centre for Medium-Range Weather Forecasts (ECMWF). It has high spatial and temporal resolution and provides mean hourly wind speeds at two heights (10 m and 100 m) above ground level (a.g.l.). The reanalysis ERA5 data are available online for public download. One of the advantages of these reanalysis data is that they cover periods of many years of historical data. It is proposed to use machine learning (ML) techniques to estimate the wind resource at the hub height of the WT at the target site corresponding to the years considered in the study (Fig. 4). This task is developed in Subsection 2.2.1.

The second task (Fig. 4) consists of initial estimation of the *NWT* required to cover annual freshwater demand, considering an SWRO plant SEC range. For each SEC, the *NWT* of the selected WT must be able to cover the annual water demand based on the wind data from the year with the least wind power. Similarly, the *NWT* must also be able to cover the on-grid system energy self-consumption [36,42]. This task is developed in Subsection 2.2.2.

The optimization process is undertaken in the third task (Fig. 4). For a given SWRO plant capacity *Qm* (m^3/day), with an associated SEC (kWh/m^3), a search is undertaken of the *NWT* and BESS size required in each of the considered wind years to cover the annual water demand and satisfy the energy self-consumption of the proposed system.

The specific cost, C_s (€/m^3), of the product water with each configuration is estimated. For this, the investment costs of the subsystems which make up the configurations (*NWT*, SEC, *Qm* and BESS capacity) are taken into account, as well as the operating and maintenance (O&M) costs. The latter may include the off-site power purchase agreement (PPA) [46], in other words the costs associated to a long-term purchase agreement between a renewable developer and a marketer who will resell the energy.

The estimated lifetime, *L*, and the discount rate, *I*, are considered to estimate the *Cs*. This third task is developed in Subsection 2.2.3.

2.2.1. Task-1. Estimation of long-term wind speed at the target site

Fig. A.1 shows a synthesised schematic representation of the first task. In each year *i* and time step *j* (hours), the variables v_x and v_y are read, extracted from the ERA5 dataset [39]. The subindices *x* and *y* are the longitude and latitude components of the ERA5-registered wind speed at 100 m a.g.l.. Based on these components, for each year *i* and hour *j*, the $V\_100_{i,j}$ wind speed module and its direction $\Theta\_100_{i,j}$ are determined. Sequencing was performed in the R programming language. $\Theta\_100_{i,j.}$ takes the value of 0° in the case of N winds and a clockwise direction is followed. The atan2($-v_x$,-v_y) function in R is used to calculate $\Theta\_100_{i,j.}$, and if $\Theta\_100_{i,j.} < 0$ it is taken that $\Theta\_100_{i,j.} = 2\pi + \Theta\_100_{i,j.}$.

After estimating the wind speeds and directions at 100 m a.g.l. using the ERA5-based data, an ML model is trained, validated and tested. The aim is for the model to learn, in a supervised manner, the existing relationship between the ERA5 data used as input signals and the estimated short-term target site wind speeds at the hub height *h*, *VT_h*, of the selected WT. In the model proposed in this study, Eq. (1), one of the input variables is the ERA5-registered wind speed at 100 m, *V*_100. As also undertaken in other studies [32,44,45], the wind direction signal, θ_100, registered in ERA5 at 100 m, is decomposed into its sine and cosine components, and the angle corresponding to the northerly direction is taken as angle 0°.

The aim with the variables of month (*M*) and hour *(H)* is to include seasonal and daily wind behaviour. In this work, the regression function given in Eq. (1) is estimated using the Random Forest (RF) technique proposed by Breiman [47]. It has been concluded in previous studies that this technique provides appropriate metrics when compared to other ML techniques [33,48,49]. It was selected for the present study in view of its robustness against overfitting.

$$(VT\_h)_t = f\left\{(V\_100)_t, cos\left[(\theta\_100)_t\right], sin\left[(\theta\_100)_t\right], M_t, H_t\right\} \quad (1)$$

The randomForest package [50] of the open-source multi-platform R Statistics software [51] was used to programme the proposed model. Model tuning via grid search was used to estimate the hyperparameters of the RF model. The tune_grid() function computes a set of performance metrics for a pre-defined set of tuning parameters (number of trees (ntree), number of features considered at each split (mtry) and maximum tree depth (max.depth)) that correspond to a model. Ntree is set in this work in the range of 500 to 4000, mtry in the range of 1 to 5 (the total number of features) and max.depth in the range of 10 to 60.

The estimated wind speed data at hub height *h* of the WT at the target site and the ERA5-registered data corresponding to the same period are divided into two subsets: one, comprising 80% of the data, for model training and validation, and the other, comprising the remaining 20%, for model testing.

If the available short-term target site wind speeds are registered at a height h_r below the height *h* of the hub of the WT, use is proposed of a log law model which, based on meteorological theory, has generally been employed considering that the boundary layer is neutrally buoyant [52]. In Eq. (2), z_0 is the surface aerodynamic roughness length, a parameter that is a representative value of surface characteristics [53].

$$(VT\_h)_t = (VT\_h_r)_t \cdot \frac{Ln\left(\frac{h}{z_0}\right)}{Ln\left(\frac{h_r}{z_0}\right)} \quad (2)$$

Use is also proposed of the 10-fold cross-validation method, which provides a robust estimation of the generalization error. The vfold_cv() function available in the rsample package [50] of the R Statistics software can be used for this purpose.

After the training and validation of the RF model with the best hyperparameters, the permutation feature importance measurement, introduced by Breiman [47] for RFs, is used to determine the most important variables to the model.

After defining the RF model, it is tested using the predict() function, available in the randomForest package [50] of the R Statistics software, and the test subset as its input data. Then, with the selected model, the long-term wind speed prediction at height *h* at the target site is undertaken. The metrics proposed to carry out the analysis are the root mean square error (RMSE), the mean absolute error (MAE) and the coefficient of determination (R^2).

2.2.2. Task-2. Estimation of the minimum number of wind turbines

To determine the minimum *NWT* that a WF requires to cover the energy self-consumption of the on-grid system and the energy consumption of the SWRO plant of capacity *Qm* and SEC, the mean annual power, $W\bar{T}PO_{min}$, is estimated that a WT of the WF would generate in the year with the lowest wind resource in the series of years considered in the study (Fig. A.2).

The power curve of the selected WT is used to calculate its power output according to the estimated wind speeds at hub height *h* in Task-1, Eq. (3):

$$WTPO_t = \frac{1}{2}\cdot\rho_t\cdot S\cdot(VT\_h_t)^3\cdot c_p(\lambda,\beta) \quad (3)$$

In Eq. (3), the power $WTPO_t$ produced by a WT in an instant *t* depends on the wind speed V_t at hub height *h*, the rotor swept area *S*, the

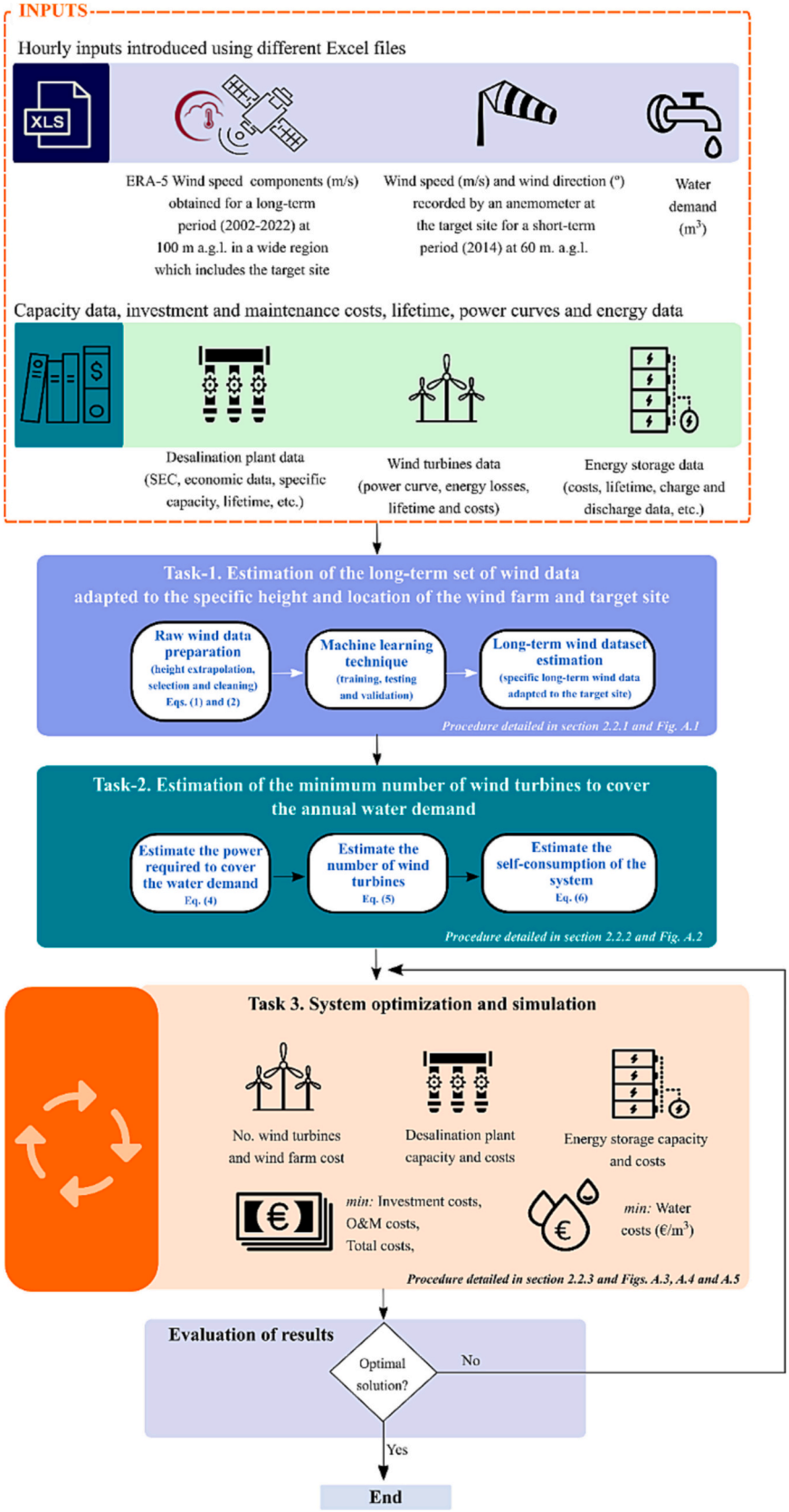

Fig. 4. Schematic representation of the method followed in this research.

air density ρ_t and its power coefficient c_p, which is a function of the tip speed ratio λ and the pitch angle β [54]. While the literature acknowledges the influence that the temporal variability of ρ_t has on estimation of the wind power density (WPD) [55] and the power curve of WTs [49], Eq. (3) is generally solved assuming that air density is constant over time, with the value used being 1.225 kg m^{-3} [56], which corresponds to standard atmospheric conditions, or the mean value, $\bar{\rho}$, estimated at hub height [57].

Currently, wind turbine manufacturers tend not to make public the power curves of their machines. Therefore, in this work a parametric model for WT power curves is used which incorporates environmental conditions, as proposed by Saint-Drenan et al. [54]. This model can be fed with the data related to rotor diameter, cut-in wind speed, cut-out wind speed, nominal power, turbulence intensity, hub height h, generator type, etc., that the WT manufacturer does provide.

The power that is required to cover the freshwater demand with the SWRO plant of Qm capacity and specific consumption SEC_i is determined through Eq. (4):

$$Pm_i = SEC_i \cdot \left(\frac{Qm}{24}\right) \tag{4}$$

The NWT_i which is required to cover the Pm_i and the losses is determined through Eq. (5), in which the ceiling(•) function returns the smallest integers larger than the parameter. In Eq. (5), L_6 is the proportion of estimated losses when transporting the wind-sourced electrical energy from the on-grid production centre to the SWRO plants, L_1 the proportion of estimated losses due to the wake effect of the WTS in the WF [53,58,59], L_2 the proportion of estimated losses due to WT unavailability [53,59], L_3 the proportion of estimated losses for environmental reasons (formation of ice and dirt on the blades) [59], L_4 the proportion of estimated losses due to technical reasons (hysteresis, parasitic load and WT rotor misalignment) [59] and L_5 the proportion of estimated losses when transporting the electrical energy from the transformer at the WF to the on-grid production centre [59] (Fig. 3).

$$NWT_i = \text{ceiling}\left(\frac{Pm_i \cdot (1+L_6)}{\bar{WTPO}_{min} \cdot (1-L_1)\cdot(1-L_2)\cdot(1-L_3)\cdot(1-L_4)\cdot(1-L_5) - \bar{SC}}\right) \tag{5}$$

$\bar{SC}$, Eq. (5), represents the rough initial estimate of the self-consumption of the system, which is considered covered by the energy generated by the WTs. The composition of $\bar{SC}$ is shown in Eq. (6):

$$\bar{SC} = \delta \cdot C_3 \cdot P_r + CSP + C_1 \cdot P_r^{C_2} + (1-\delta)\cdot C_4 \cdot P_r^{C_5} \cdot \left(\frac{\bar{WTPO}_{min}\cdot(1-L_1)\cdot(1-L_2)\cdot(1-L_3)\cdot(1-L_4)}{P_r}\right)^2 \tag{6}$$

The first term of Eq. (6) is the consumption of active power that the WTs demand to be able to feed their local control systems and the ancillary services [42] during standstill as well as in idle mode. The electrical loads that contribute to the energy consumption include the control boards, lights, communication, sensors, metering, data collection, yaw mechanism (to maintain the rotor perpendicular to the wind and also to unroll the electric cables of the tower when required [42]), blade-pitch control (adjustment of the wind turbine blades, making them turn in order to use the correct fraction of the available wind energy to obtain the greatest power output while guaranteeing that the turbine does not exceed its maximum turning speed), cooling system (tower fan, nacelle fans, converter cabinet fans), heating system (nacelle heating and dehumidification during periods of high humidity, low temperatures and low wind speed, converter cabinet heating), heating the blades in cold weather [42], and running the turbine using the generator as engine (if wind speed is varying close to the cut-in wind speed the blades are kept turning using the generator as engine because then production is more easily started as wind speed increases over the cut-in value [42]). The second term of Eq. (6), *CSP,* represents the power consumption of the control system. The third term of $\bar{SC}$ represents the no-load losses of the transformers [60] and the fourth term their on-load losses [60]. δ is the proportion of annual hours of the year under consideration in which the WTs, of rated power P_r, were inoperative. The coefficients C_1, C_2, C_4 and C_5 can be obtained from the technical specifications provided by the manufacturer [61,62]. The coefficient C_3 can be estimated from the compiled experimental data [42].

2.2.3. Task-3. System optimization

The steps to follow are as follows:

a) Step 1: Firstly, the energy storage requirements in an uninterrupted power system (UPS) for each hour of each study year are estimated (Fig. A.3).

The aim with the UPS is to deal with the energy self-consumption of the proposed on-grid system or, in other words, the power that is used by the wind turbine itself and the ancillary services in order to continue functioning even if there is no wind [63] and the energy demanded by the CS. If the WTs are operative and generating sufficient active power the aforementioned power consumption is covered by the WTs themselves.

However, in on-grid systems, during standstill as well as in idle mode (the WF does not produce electrical energy due to a lack of wind, although some relevant required loads, such as the yaw mechanism, cable unrolling, cooling and heating and the blade heating system, are active), the WTs have to consume active power from the conventional grid to feed their local control systems and ancillary services. In the case of isolated systems, diverse strategies have been proposed in the literature to avoid the use of energy from the conventional grid or auxiliary diesel generators [36].

With the input data indicated in Fig. A.3, the required hourly UPS_t are analysed for each year under consideration. For this, the starting point is the power generated each hour by the WF ($WFPO\_1_t$), integrated by *NWT*, corrected for losses L_1 to L_4. The hourly required capacities, UPS_t, of energy storage are determined according to the difference between the available wind power and the energy self-consumption of the system. Self-consumption consists of the no-load losses (*NLL_WF* and *NLL_B*) and the on-load losses (*LL_WF* and *LL_B*) of the transformers of the *WF* and the battery system.

At the same time, self-consumption comprises the powers required by the WF during standstill as well as in idle mode (*CS_WF*) and the powers demanded by the control system (*CSP*). UPS_t depends on the UPS_{t-1}, which increases by σ, the set-discharge rate in time t [64]. *RTE* is the round-trip DC-to-storage-to-DC energy efficiency of the batteries and the electronic power converters.

b) Step 2: After estimation of the *MIY*, determination is made of the maximum battery energy storage requirements ($MBAT_y$), for each study year considered, to balance the mismatches between the power $WFPO\_5_h$ generated by the WF, which is available after covering self-consumption, and the power $Pm_i \cdot (1 + L_6)$ which has to be fed into the conventional grid for consumption by the SWRO plants in each instant t (Fig. A.4).

In each instant t, battery charging and discharging is carried out (Fig. A.4) using the mathematical models shown in Eq. (7) and Eq. (8), respectively.

$$BAT_t = BAT_{t-1} \cdot (1-\sigma) + (WFPO\_5_t - Pm \cdot (1+L_6)) \cdot \sqrt{RTE}; WFPO\_5_t > Pm \cdot (1+L_6) \quad (7)$$

$$BAT_t = BAT_{t-1} \cdot (1-\sigma) - (Pm \cdot (1+L_6) - WFPO\_5_t) \Big/ \sqrt{RTE}; WFPO\_5_t < Pm \cdot (1+L_6) \quad (8)$$

c) Step 3: Following the block diagrams of Fig. A.3 and Fig. A.4, which synthesize the subroutines which determine the energy storage capacities in UPS and BAT, respectively, the wind power surpluses, which tend to increase with *NWT*, can result in the oversizing of these capacities, which must be delimited. In this context, Fig. A.5 shows a block diagram of the subroutine used to try to limit the two aforementioned energy storage capacities in each study year. In the case of BAT, the subroutine of Fig. A.5 reduces (while $Out = 0$) the maximum storage capacity obtained with the subroutine shown in Fig. A.4 until the minimum charge (min(BAT)) is between 0 and a value accepted as tolerable (Tol) (see, by way of example, Fig. 5). In the UPS case, the subroutine of Fig. A.5 reduces (while $Out = 0$) the maximum storage capacity obtained with the subroutine shown in Fig. A.3, until it reaches the maximum admitted depth of discharge (DOD), with a certain tolerable error (Tol). That is, until the minimum charge (min(UPS)) implies that the state of charge (SOC) = (100-DOD)% of the maximum charge (see, by way of example, Fig. 6).

d) Step 4. Calculation of the specific cost of the water produced with each configuration of the system. After saving in the vectors MUPS and MBAT the energy storage capacities for each study year (Fig. A.5), their maximum values (max_*UPS* and max_*BAT*) are selected. In the case of max_*BAT*, its value is modified to delimit its DOD, Eq. (9).

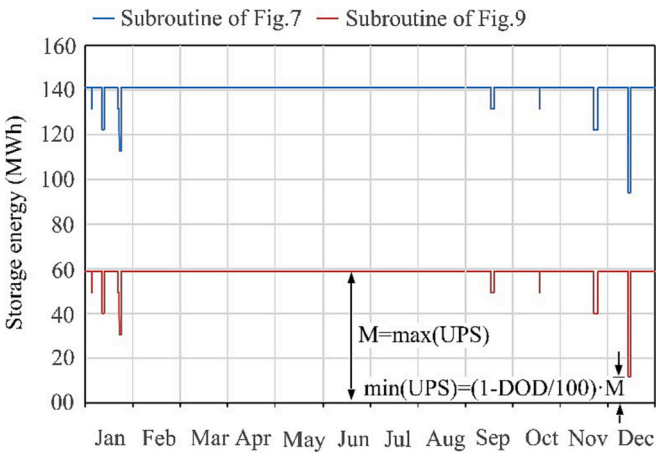

Fig. 6. Example of delimitation of the maximum UPS-stored energy capacity during one of the years considered in the present study.

$$max\_BAT = \frac{max\_BAT}{DOD} \cdot 100 \quad (9)$$

For each system configuration, defined by the values of the variables Qm, SEC, NWT, max_UPS and max_BAT, an analysis is undertaken of the specific cost per m^3 of product water in each one.

In this study, to select the optimal configuration from an economic perspective, it is proposed to use the simplified cost of water (SCOW) method [65], Eq. (10), which has been widely used in the literature.

In Eq. (10), *TPV* is the total present value of the actual cost of all the subsystems of a given configuration. That is, *TPV*, Eq. (11), takes into account the costs associated with the investments that need to be made in the electrical energy generation subsystem (C_{WF}), the water desalination subsystem (C_{SWRO}) and the energy storage subsystem ($C_{BESS}^{I\&R}$) [33], with the latter representing the initial investment costs C_{BESS} and the replacement costs C_{BESS}^{R}. Annual O&M costs cover the costs associated with the operation and maintenance of the system, Eq. (12).

$$TPV = C_{SWRO} + C_{WF} + C_{BESS}^{I\&R} \quad (11)$$

$$\text{Annual O\&M costs} = C_{SWRO}^{O\&M} + C_{WF}^{O\&M} + C_{BESS}^{O\&M} + \psi \cdot C^{sp} \quad (12)$$

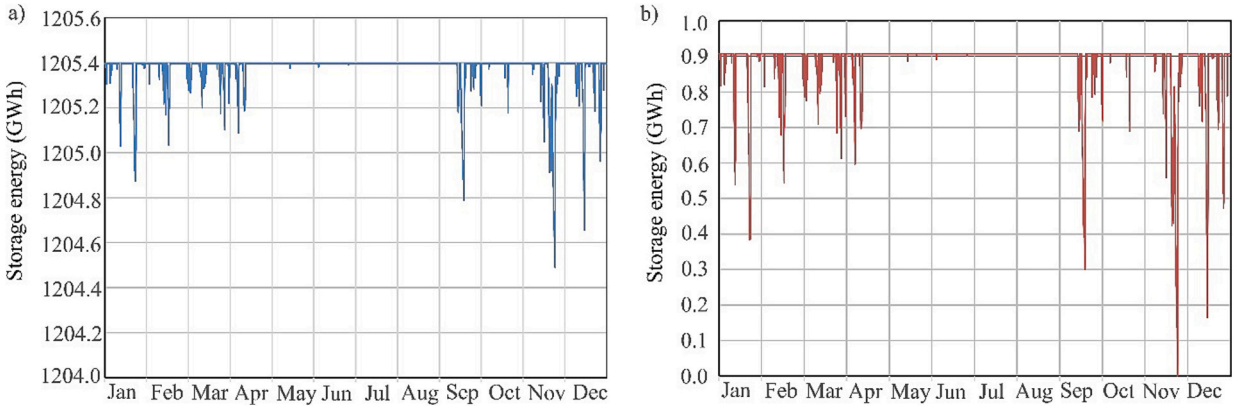

Fig. 5. Example of delimitation of the maximum battery-stored energy capacity during one of the years considered in the present study. a) Maximum capacity obtained with the subroutine described in Fig. A.4. b) Maximum capacity estimated with the subroutine described in Fig. A.5.

$$SCOW = \frac{TPV \cdot CRF + \text{Annual O\&M costs}}{Qm \cdot 365}; \text{in } € \Big/ m^3 \quad (10)$$

C^{sp} represents the costs associated to the injection of electrical energy in the conventional grid and the discharge from the grid to cover the demand of the SWRO plants; $\psi = 1$ in the case of an on-grid system and $\psi = 0$ in the case of an off-grid system.

$$C_{BESS}^{I\&R} = C_{BESS} + C_{BESS}^{R} = C_{BESS} + \underbrace{C_{BESS} \cdot \left[\frac{1}{(1+i)^{y_1}} + \frac{1}{(1+i)^{y_2}} + \cdots \right]}_{C_{BESS}^{R}} \quad (13)$$

In Eq. (13), C_{BESS}^{R} depends on the periods y_1, y_2, …, in which battery replacement is made, and the discount rate, i, that is used, which represents to a certain degree the opportunity cost of the resources employed [33,66,67].

The *CRF*, Eq. (14), is the capital recovery factor, which is dependent on the useful life, L, of the system and the discount rate, i.

$$CRF = \frac{i \cdot (1+i)^{L}}{(1+i)^{L} - 1} \quad (14)$$

3. Case study: Gran Canaria island

The Canary Archipelago is divided into two provinces: Las Palmas and Santa Cruz de Tenerife (Fig. 7).

The Canary Islands Government, in view of the insular nature of the archipelago and its subtropical-outermost region situation, issued a declaration of climate emergency in August 2019 [68].

3.1. Installed capacity of the desalination systems

The climate reality of the Canary Islands is closely related to the absence of rains. Given the additional overexploitation of its aquifers, one of the most serious problems facing the archipelago is its limited water resources.

Over the last 40 years, the installation of a rising number of desalination plants has had the aim of countering the effects of the above. In the opinion of [5], the Canary Islands can be considered pioneers in the development of desalination technology, and were, are and will continue to be a true desalination laboratory. According to [69], a total amount of freshwater of 501,735,000 m^3 was available in 2018, with 54.12% of that total being treated and purified. The volume of water for human consumption was 136,016,000 m^3, 90.50% of which came from desalination plants, 3.9% groundwater and 5.6% surface water.

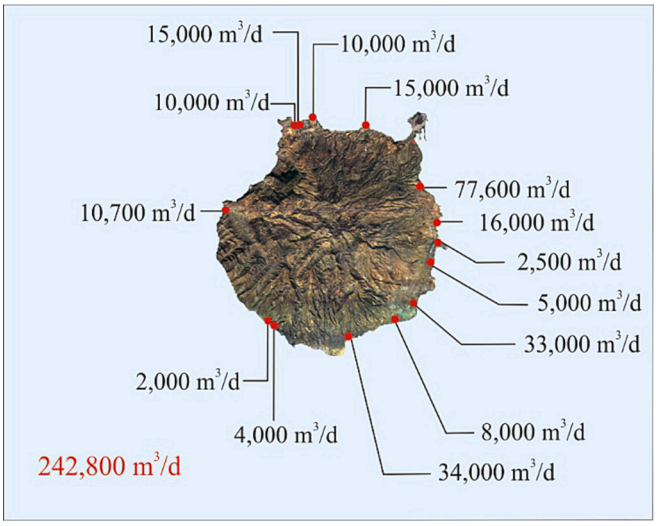

Fig. 8. Installed capacities of the most important SWRO plants on the island of Gran Canaria.

The majority of the freshwater production centres are situated in the province of Las Palmas, and more specifically the island of Gran Canaria, which, for this reason, was selected as the case study in the present paper. Fig. 8 shows the distribution of the most important desalination SWRO-based centres installed on the island and their daily production capacity. Their total installed capacity adds up to 242,800 m^3/d. The mean SEC value of these SWRO plants is, according to [70], 3.5 kWh/m^3.

3.2. Energy situation

The archipelago completely lacks conventional energy sources and there are six small-sized isolated systems with weakly intermeshed electrical infrastructure networks (Fig. 9). According to [71], the gross total power of the generator sets installed in the thermal power plants of the island at the end of 2021 amounted to 999,180 kW (Fig. 9). In that year, the majority of the total greenhouse gas emissions came from the energy sector, with the electrical energy subsector responsible for a

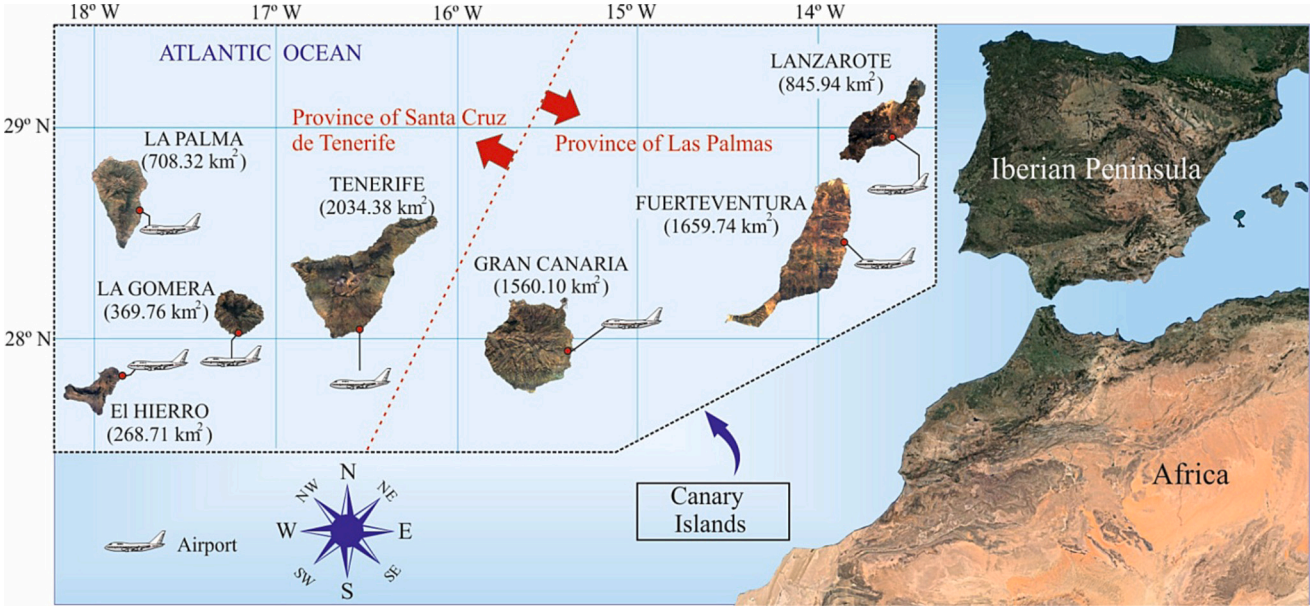

Fig. 7. Location of the case study.

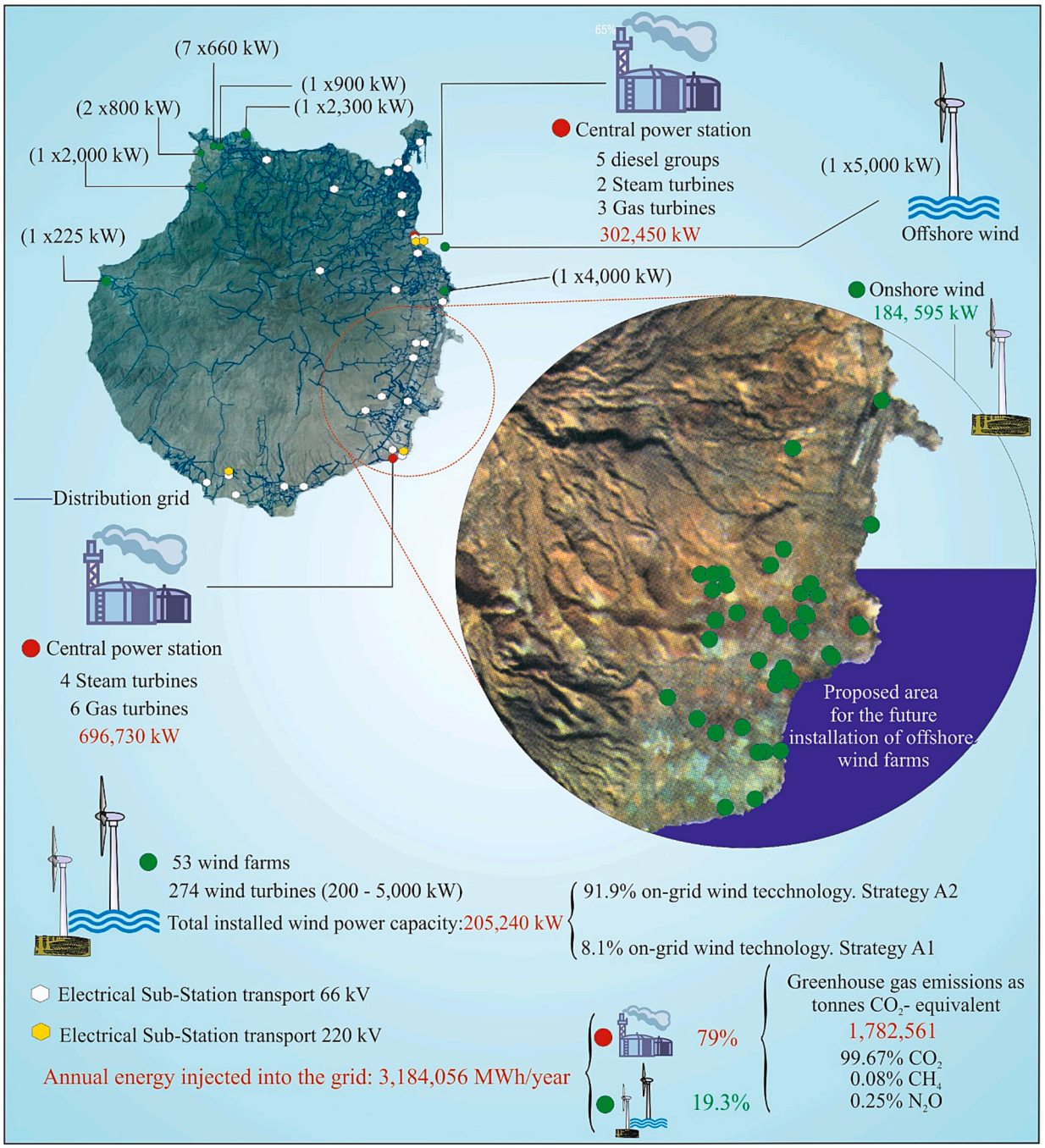

Fig. 9. Location of the thermal power plants and wind farms on the island of Gran Canaria.

significant percentage of them [71], corresponding to 1,782,561 t of CO_2-equivalent (Fig. 9). To mitigate this problem, the islands have undertaken a policy promoting the use of renewable technologies, especially in relation to wind energy. The amount of energy fed into the conventional grid in 2021 was 3,184,056 MWh, with the contribution of wind energy amounting to 19.3% [71] (Fig. 9). Most of the WTs installed in Gran Canaria are found in the southeastern area (Fig. 9), given the higher intensity of the NE trade winds that blow there.

Given the restrictions on onshore wind energy expansion because of spatial limitations [72], offshore WFs have begun to be installed off the southeast coast of the island (Fig. 9). As a result of bathymetric restrictions [73], most of the proposals that have been made are for the installation of floating WTs [74,75].

3.3. Description of the data used

For the purpose of this study, we used the mean hourly wind speed and directions available in ERA5 climate reanalysis datasets [39] in the offshore zone of UTM coordinates 27°48′02”N, 15°18′51”W. The ERA5 data used correspond to a height of 100 m a.g.l. during the period 2002–2022. In order to fit the ERA5 data to the wind behaviour of the zone, use was made of the available mean hourly wind speeds recorded at 60 m a.g.l. during 2014 by an anemometer tower situated on the southeast coast of the island at a distance of 11 km from the ERA5 point. To extrapolate the wind speeds from 60 m to 140 m (estimated hub height of the WTs), Eq. (2) was used with a constant ocean surface roughness coefficient of $z_o = 0.0002$ m [76].

The power curve of the WTs was modelled [54] using a rotor

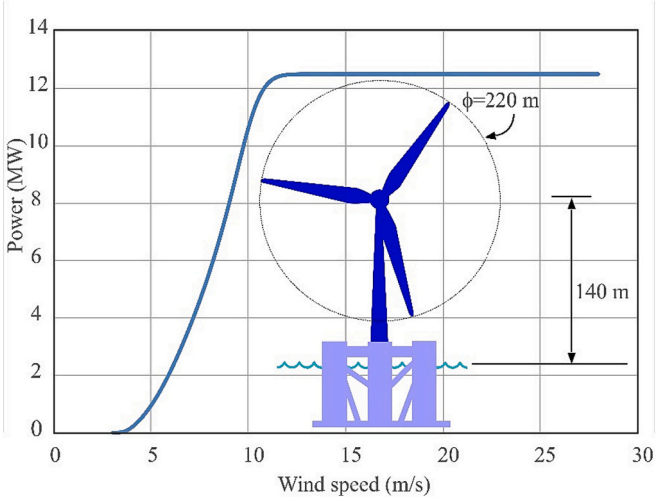

Fig. 10. Electrical power curve (corresponding to an air density of $\rho_0 = 1.225$ kg m^{-3}) of the WTs considered in this study.

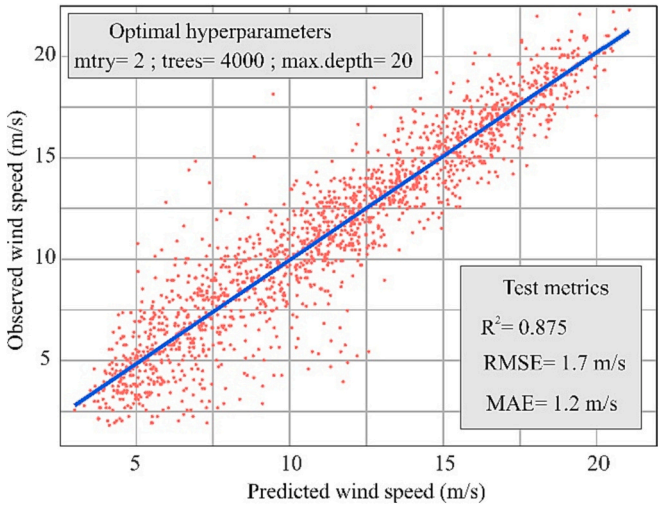

Fig. 11. Optimal hyperparameters of the RF model and the values of the metrics used in their evaluation.

diameter of 220 m, a rated power of 12,500 kW, a cut-in wind speed of 3 m/s, a cut-out wind speed of 28 m/s, an air density of 1.225 kg/m^3, a 6% turbulence intensity, and a maximum c_p of 0.42 (Fig. 10).

The total investment cost (€) in the wind farm was estimated based on the fact that the values for specific investment costs depend fundamentally on the distance from the coast, the substructure technology employed and the total installed wind farm power. According to [59], in the case of floating offshore WFs the specific investment cost would be 4200 €/kW, giving a $C_{WF} = 4200{\cdot}12{,}500{\cdot}NWT$. The annual O&M cost of the generation system was taken as 3% of the investment cost [59]. That is, $C_{WF}^{O\&M} = 0.03{\cdot}C_{WF}$. C^{sp} was estimated based on the data that the electricity market operator designated to manage the daily and intra-daily market in the Iberian Peninsula provides and on the electricity tariffs data in 2022 for large consumers (tariff 6.2TD). This tariff has 6 different hour-based energy and power periods (P1, P2, P3, P4, P5 and P6) and so the cost of both energy and power differs depending on the period when it is used [77]. Additional information can be found in the Supplementary Material (Supplementary S.1: Electricity tariffs in the Canary Islands). The types of energy losses considered and their values are as follows [59]: $L_1 = 0.05$, $L_2 = 0.05$, $L_3 = 0.005$, $L_4 = 0.012$, $L_5 = 0.036$ and $L_6 = 0.047$ [71]. The parameters used to estimate the system's energy self-consumption are: $C_3 = 0.03$ [42], $C_1 = 0.0132$, $C_2 = 0.7354$, $C_4 = 0.0292$, $C_5 = 0.8043$ [62] and $CSP = 5$ kW. Additional information can be found in the Supplementary Material (Supplementary S.2: Technical specifications of transformers).

The BESS investment cost was estimated based on the specific cost, whose value of 297€/kWh was obtained from [78]. C_{BESS} includes the cost of the PCS, balance of plant (BOP) and construction and commissioning. The useful life before replacement was estimated as 10 years. $C_{BESS}^{O\&M}$ was estimated considering a fixed cost of 6.6 €/kW and a variable cost of 0.025 cent€/kWh [78]. An RTE of 86% was assumed as well as equal charging and discharging efficiency. It was also taken that $\sigma = 0.02\%$ [79] and DOD = 80% (that is, the minimum SOC = 100-DOC is 20%).

The specific costs of the SWRO desalination plants were assumed to vary depending on their capacity. Given that SWRO plants of different capacities are being considered (Fig. 14), a mean specific cost was used of 1165 €/m^3/d weighted by the different capacities. Thus, $C_{SWRO} = 1165{\cdot}$ 242,800 m^3/d. The annual O&M costs are expressed by Eq. (15) [33]:

$$C_{SWRO}^{O\&M} = 0.106{\cdot}Qm{\cdot}365 + 0.04{\cdot}C_{SWRO} \quad (15)$$

In this work, L was estimated at 20 years and i at 5% of investments at constant prices, Eq. (14).

4. Results

The results obtained in the different tasks indicated in Fig. 4 are presented and analysed in this section.

4.1. Task-1. Long-term wind speed estimation results

It can be deduced from the analysis of the results obtained that the proposed RF model, with the three hyperparameters indicated in Fig. 11, was able to estimate the behaviour of the wind at the target site at 140 m a.g.l. with a relatively good goodness-of-fit.

All the variables used as RF model inputs contributed in reducing the forecasting error of the variable wind speed at the target site at 140 m a.g.l.. Among these variables, the ERA-based wind speed at 100 m height a.g.l. (V_100) showed the greatest importance [47] (Fig. C.1). This was expected given the high correlation existing between V_100 and the wind speed at 140 m a.g.l. at the target site. Additional information can be found in the Supplementary Material (Supplementary S.3: Results of Task-1).

As can be seen in Fig. 12, the mean daily behaviour of the wind at 100 m a.g.l., according to the data registered in ERA5, differs from the mean daily observed wind behaviour at 60 m a.g.l. in the target area.

The profile generated with the ERA5 data shows higher wind speeds

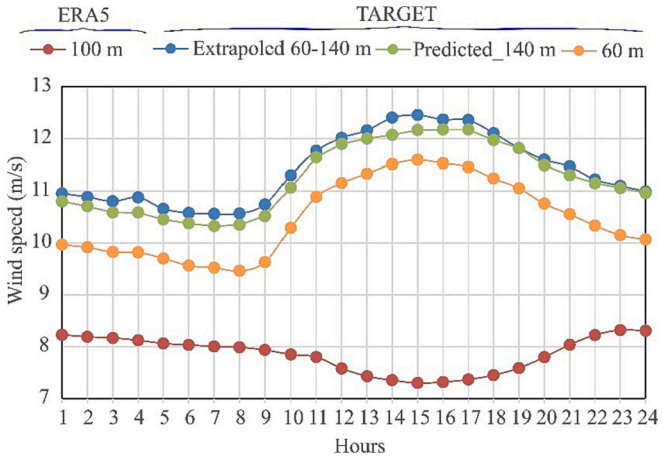

Fig. 12. Mean daily wind speed profile registers in ERA5 at 100 m height and at the target site at 60 m a.g.l., and mean daily wind speed profile extrapolated and estimated at the target site at 140 m a.g.l..

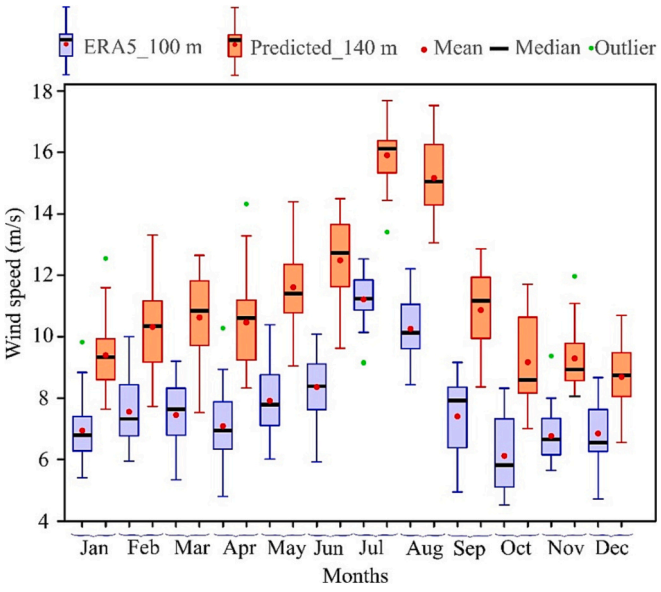

Fig. 13. Boxplot of the mean monthly ERA-registered wind speeds at 100 m a.g.l. and mean monthly wind speeds at 140 m a.g.l. at the target site estimated with the RF model for the study period (2002–2022).

occurring during the night. However, the typical profile of the zone shows the wind speeds falling at night and tending to reach their highest values between 12:00 and 18:00. One of the benefits of the proposed RF model is its ability to fit the ERA5-based wind profile, which is not characteristic of the zone, to its typical actual wind profile.

Fig. 13 shows a boxplot of the mean monthly estimated wind speeds at 140 m a.g.l. and of the mean monthly ERA5-registered wind speeds at 100 m a.g.l at the target site. A certain trend can be seen in the seasonal behaviour of the wind. Given the influence of the trade winds in the area, the wind speed tends to increase in the summer months of June, July and August.

Additional information can be found in the Supplementary Material (Supplementary S.3: Results of Task-1).

4.2. Task-2. Results obtained in the estimation of the minimum number of wind turbines

According to the results obtained in Task-2, a total of 5 WTs is sufficient to cover, in the year with the lowest wind intensity, the annual energy that needs to be fed into the conventional grid (324.76 GWh/year) to cover transport losses and meet the demand of the SWRO desalination plants in the case that the latter operate with a SEC of 3.5 kWh/m^3. That is, with 5 WTs connected to the grid and operating in accordance with the A-1 strategy described in Subsection 1.1.1, it is possible to cover the estimated annual desalinated water demand of 88.622 Hm^3/year. Based on the initial technical and economic data considered in the present study, the specific cost of the wind energy that needs to be fed into the conventional grid is 0.09 €/kWh. It should be noted that with 5 WTs it is also feasible, according to the estimations made through Eq. (5), to cover the self-consumption of the system in the scenarios in which the SECs of the SWRO plants are in the range from 3 to 3.5 kWh/m^3. However, up to 6 WTs are required if the SECs are in the range from 3.6 to 4.2 kWh/m^3.

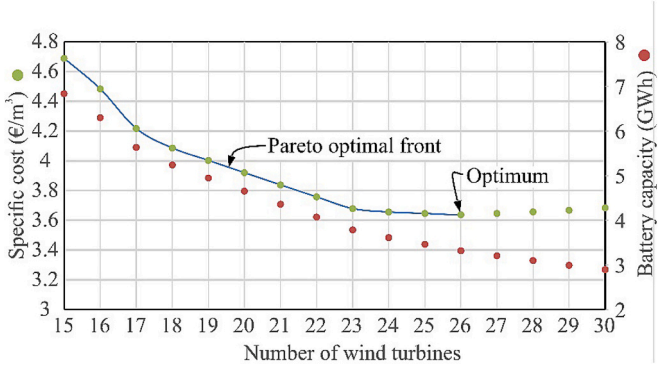

Fig. 14. Specific costs of the product water according to the number of wind turbines and BESS capacity for a specific energy consumption of the SWRO plants of 3.5 kWh/m^3.

4.3. Task-3. System optimization results

As Fig. 14 shows, as NWT increases the required BESS capacity falls until reaching the optimal value according to the Pareto optimal front. As can be seen in Fig. 14, in the case of considering a SEC of the SWRO plants of 3.5 kWh/m^3, 26 WTs are required and a BESS capacity of 3.32 GWh. This capacity is distributed as follows: 10.2% (340 MWh) in the capacity of the UPS which has to supply power to the CS and ensure that the power required by the different devices of the WTS and the ancillary services of the proposed on-grid system is covered in the periods in which there is insufficient wind energy available; and 89.8% (2.98 GWh) to balance in each instant the mismatches between the power demand of the SWRO plants and the WF-generated power. If the BESS is comprised of packs of 3 MWh, a total of 1107 units will be required. If the recommended area [80] for the installation of each of these units is considered, the approximate surface area that these 1107 units will occupy is 4.3 Hm^2. Additional information can be found in the Supplementary Material (Supplementary S.3: Results of Task-1).

Fig. 15 shows a simulation of the optimal configuration of the system during the study period (2002–2022) in which can be seen the capacity of the BESS required to balance in each instant the mismatches between the power demand of the SWRO plants and the WF-generated power (Fig. 15a) and the required capacity of the UPS (Fig. 15b), such that the maximum discharge does not exceed 80% in any given moment (minimum SOC = 20%). The most frequent SOCs are in the 80%–100% range. The SOC frequencies below 60% are very small, but nonetheless cause the required BESS capacities to be high.

The investment and O&M costs that are shown in Table 1 result in a minimum specific cost of the energy consumed by the SWRO plants of 0.82 €/kWh (excluding taxes) and a specific desalinated water cost of 3.64 €/m^3.

As shown in Fig. 16, the SECs of the SWRO plants have a direct effect on the specific cost of the energy consumed and, consequently, on the cost of the desalted water. If the SEC of the SWRO plant can be reduced from 3.5 kWh/m^3 to 3 kWh/m^3, the specific cost of the product water is lowered by 12.4% and the footprint generated by SWRO plant energy consumption that must be eliminated is reduced by 14.28%.

Fig. 17 represents the results obtained after carrying out a sensitivity analysis to identify the impact on the initial results of certain changes to the variables (investment costs and O&M costs). In Fig. 17A and B, the impact is shown on the specific cost of water (€\m^3) and the specific cost of energy (€/kWh), respectively, when reducing in percentage terms the investment costs of the different subsystems that participate in the analysed whole. More specifically, the effect of reducing the investment costs of the WF, the BESS and the SWRO is analysed along with the combined effect produced by the reduction in costs of the WF together with the BESS when the useful life of the latter is increased to 20 years. Also, in orange, the combined effect of increasing the useful life of the BESS to 20 years and reducing its cost can be observed. Fig. 17C and D show the impact on the two parameters when reducing in percentage terms the O&M costs of each of the subsystems (WF, BESS and SWRO).

Bearing in mind that this research article focuses on offshore wind energy, Table 3 summarizes the number of jobs created during the construction phase and during the O&M phase assuming two scenarios

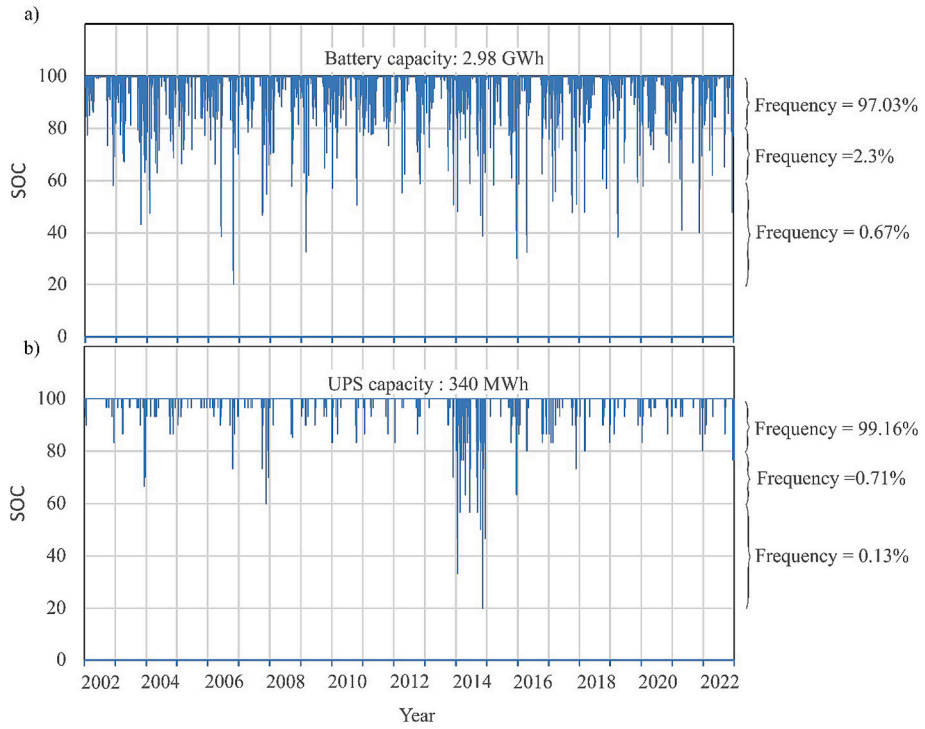

Fig. 15. Hourly SOC for the optimal configuration for each of the 21 years (2002–2022) considered in the study: a) BESS used to balance in each instant the mismatches between the power demand of the SWRO plants and the WF-generated power. b) UPS used to cover the self-consumption needs of the system.

Table 1
Costs of the optimal system.

Investment			O&M			Cost	
WF M€	SWRO M€	BESS M€	WF M€	SWRO M€	BESS M€	Water €/m^3	Energy €/kWh
1365	282.86	1561.70	40.95	20.71	19.68	3.64	0.82

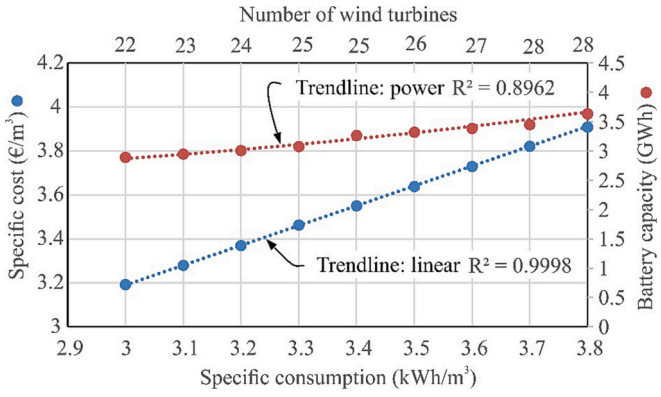

Fig. 16. Specific product water cost depending on the SEC of the SWRO plants.

in which 20 and 23 offshore wind turbines of 12.5 MW each are installed, respectively. As shown in Table 3, the total number of jobs created as a result of the implementation of the proposed schemes (almost entirely during the construction phase) would vary, according to the International Renewable Energy Agency data, in a range between 4322 and 4971 jobs.

5. Discussion

The interesting result obtained in Section 4.1 (see Fig. 12) induces us to recommend, to the extent that it is possible, not to make direct use of ERA5 reanalysis data, but instead to use ML techniques to fit these data to the actual wind profile in the study area. This fitting is important given that it will influence calculations of the amount of energy generated by the WF that is injected each hour directly in the conventional grid, the electricity tariffs and the sizing of the BESS.

In Fig. 13, it can be seen that the mean wind speed interannual variation in a particular month can present significant differences and atypical values (outliers). In this context, it is recommended to discard the use of models which only use one series of annual wind speed data. With a view to obtaining a more robust model, there is a need to consider the interannual and seasonal evolution of wind speed when evaluating the proposed on-grid wind energy system (WF and BESS) for water desalination.

According to Section 4.2, the specific cost of the wind energy that needs to be fed into the conventional grid is 0.09 €/kW. This specific cost is in concordance with the values estimated for the Atlantic European coast, which presents, as does the study zone in the present paper, a high wind resource in terms of energy production [81]. This cost is relatively low, however, due to the lack of synchrony between the energy fed into the conventional grid and the demand of the SWRO plants, which also require fossil fuel-sourced energy.

Additionally, according to the results obtained in Task 3 (see Section 4.3), in order to obtain a minimum product water specific cost such that there is synchrony between the wind-sourced energy fed into the conventional grid and the consumption of the SWRO plants, it is necessary to substantially increase the size of the WF mentioned in the previous section and decrease the capacity of the BESS. This is a consequence of the high cost of the BESS in relation to the cost of the WF and of the replacement costs C^{R}_{BESS} that arise during over the course of the system's lifetime.

In Section 4.3 it was found that the most frequent SOCs are in the 80%–100% range. The SOC frequencies below 60% are very small, but nonetheless cause the required BESS capacities to be high. These SOC frequencies corroborate the highly limited large discharges of the BESS and, therefore, the highest percentages of power fed each hour into the

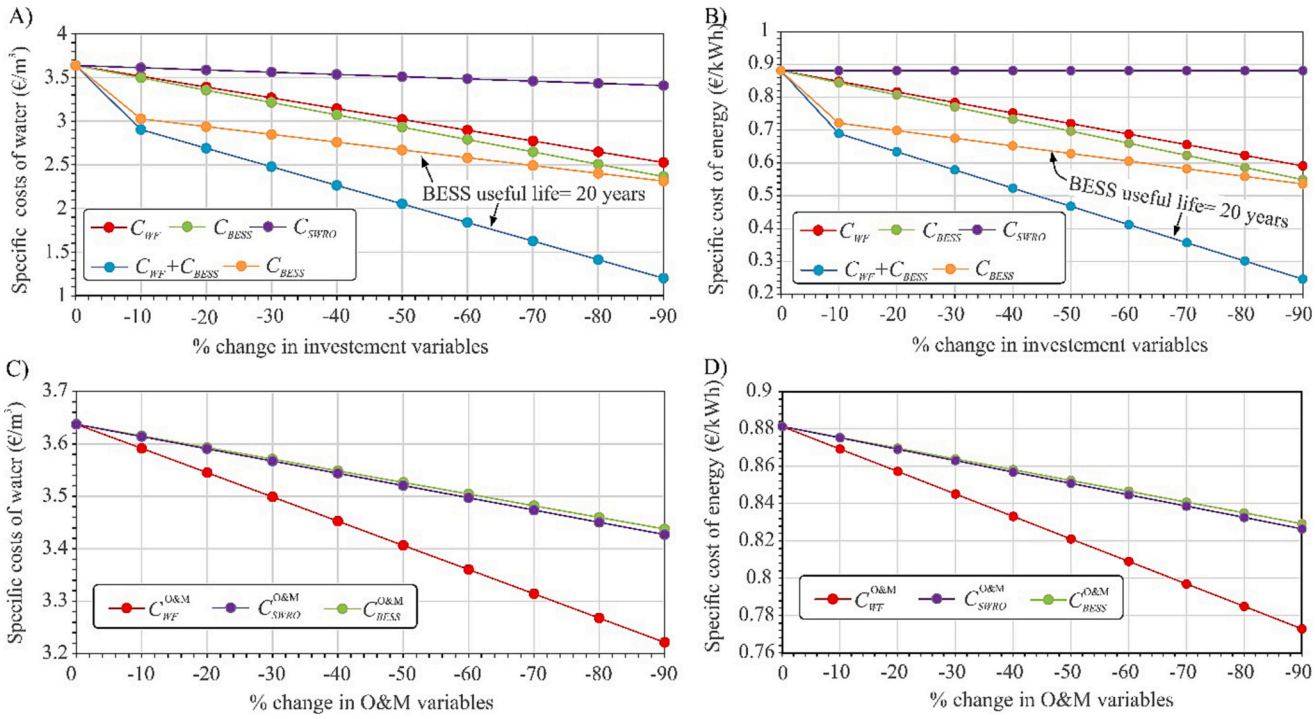

Fig. 17. Spider diagram representing the sensitivity analysis carried out in the study.

conventional grid come directly from the WF. It should be noted that an interannual analysis of the wind data series, as proposed in the present paper, is required to detect the situations in which the DODs are high. The analysis should not be limited to the data series of a single randomly chosen year, nor should a mean year be used. It is also concluded that, in the case of the BESS (Fig. 15a) used to balance in each instant the mismatches between the power demand of the SWRO plants and the WF-generated power, the capacity of the BESS could be reduced if the shutdown of certain SWRO plants is accepted in periods in which the SOCs tend to be very low. If these shutdown periods are not very long, this action would not necessarily affect the water supply as SWRO plant facilities usually have product water regulating reservoirs.

As can be seen in Table 1, the product water energy cost is 3.5 kWh/m^3·0.82 €/m^3 = 2.87€/m^3. However, the energy cost of the SWRO plants connected to the conventional grid, with the 6.2 TD tariff and excluding taxes, is 3.5 kWh/m^3·0.115€/kWh = 0.4025 €/m^3. That is, the energy cost of a cubic metre of desalinated water with the system proposed in the present paper is 7.1 times higher than the cost generated by the SWRO plant if it is powered from the conventional grid. However, with the proposed system, if a SEC of 3.5 kWh/m^3 and an installed SWRO capacity of 242,800 m^3/day are considered then an annual reduction of the emission of 219,915.5 t CO_2 equivalent (tCO2eq) is achieved. This is equivalent to eliminating 4,398,310 tCO_2-eq during the 20-year lifetime of the system. In this case, each avoided tCO_2_eq has an associated cost of 1156.6 €. At this point it should be noted that, although the proposed system substantially reduces the carbon footprint generated by the energy used and contributes to the fight against climate change, a carbon footprint nevertheless remains when taking into account the complete life cycle of the system, made up of the WF, the BESS and the SWRO plants. According to studies carried out by García-Teruel et al. [82], in the case of floating offshore structures, the mean emission range is 34.25 gCO_2 eq/kWh. According to the life cycle assessment (LCA) of lithium-ion batteries carried out by Yudhistiva et al. [83], their impact would be 0.9 $kgCO_2$ eq/kWh delivered. Najjar et al. [84], in an LCA study that they undertook with SWRO plants, estimated that the emissions would be 0.36 $kgCO_2$ eq per m^3 of product water. Based on the above studies, we estimate that the carbon footprint over the lifetime of the proposed system that cannot be reduced despite the proposed operating strategy would be 1,285,660 tCO_2 eq. Of this footprint, 23.37% (30,052,000 tCO2 eq) is from the SWRO plants and the remaining 76.63% is due to inclusion of the WF and the BESS. Therefore, the LCA footprint percentage eliminated from the system would be: 4,398,310·100/(4,398,310 + 1,285,660) = 77.4%.

As previously mentioned, the optimal system configuration depends heavily on the specific cost of the BESS and the replacement costsC^{R}_{BESS}. If, given the significant size of the analysed system (1107 packs of 3 MWh each) [85], a 16% reduction in the considered specific cost of the BESS (297 €/kWh) and a BESS useful lifetime of 20 years (instead of the 10 considered in the present study) were feasible, the resulting configuration would be different (Table 2). The number of WTs would be reduced by 15.38% (from 26 to 22), while the BESS capacity would increase by 14.16% (from 3.2 to 3.79 GWh). The NWT reduction would have an associated variation in the SOC of the BESS such that the frequency of the SOC range of 20%–80%, indicated in Fig. 16a, would increase by 33.67%.

This increase in large discharges indicates an increase in the percentage of BESS participation in the power that is injected into the conventional grid each hour and, consequently, a decrease in the power directly injected by the WF. The product water specific cost is reduced by 19.78% (from 3.64€/m^3 to 2.92 €/m^3). If the SWRO plants had a SEC of 3 kWh/m^3, a cost of 2.57 €/m^3 could be achieved. However, this cost is still 6 times higher than the cost which, according to Karagiannis and Soldatos [86], is generated in SWRO plants with capacities ranging

Table 2
Optimal system configuration: BESS useful life = 20 years, BESS specific cost = 249.48 €/kWh.

SEC	NWT	BESS capacity	Avoided CO_2-eq	Non-avoided CO_2-eq	Cost	
kWh/m^3		GWh	tonnes	tonnes	Water €/m^3	Energy €/kWh
3	20	3.17	3,770,231	1,355,043	2.57	0.632
3.5	23	3.79	4,398,310	1,516,197	2.92	0.634

Table 3
Number of jobs created during the construction phase and during the O&M phase. Source: [B.6] [B.8].

Wind turbine nominal power (MW)	Number of wind turbines	Jobs created during the construction phase (jobs/MW installed)	Jobs created during the O&M phase (jobs/MW installed)	Estimated total number of jobs created
12.5	20	17.29	Negligible	4322
12.5	23	17.29	Negligible	4971

between 100,000 and 300,000 m^3/day that use conventional energy.

It can be concluded from the sensitivity analysis shown in Fig. 17 that the reduction in investment costs in the BESS and the WF have the greatest impact on the specific cost of water the specific cost of energy. The combined effect of both reductions, together with the potential increase in the useful life of the BESSs could result in the costs being similar to those currently attained with fossil fuel-powered desalination plants. For its part, reductions in O&M costs in the different subsystems have a lower impact in terms of lowering the specific water and energy costs. However, reductions of the O&M costs of the WF do have greater impact than those of the BESS or SWRO.

Additionally, it should be noted in Table 3 that the number of jobs created per MW of installed wind power varies significantly with respect to the maturity of the technology. Specifically, in scientific and grey literature between 2009 and 2015 it was common to find values of direct job creation per MW of installed wind power varying in a range between 10 [87], 15 [88], 20 [89] and up to 27 jobs per MW installed [90]. In terms of jobs created during the O&M phase, these were in the range of 0.7 [90] to 1.5 per MW installed [88]. However, the post-2020 scientific literature is much more restrained in this regard. Specifically, the number of direct jobs created during the construction phase of an onshore project would vary from 4.9 [91], 5.24 [92] to 5.66 per MW installed [93]. As for the number of direct jobs per MW of installed offshore wind energy, these would amount to 17.29 jobs per MW [92]. Regarding the number of jobs created during the O&M phase, the post-2020 literature shows a limited impact on job creation (0.056 jobs per MW installed) [94].

Finally, it should be noted that to replicate this method in a given geographic location the wind resource data need to be available in ERA5 for a long time period, given the spatio-temporal variability of the wind resource in different regions. In this way, applying the methodology indicated in Section 2 of the paper, the replicability of the first task of the method is guaranteed. Likewise, a wind device needs to be selected and the power it can generate calculated using the software specified in the manuscript. Calculation also needs to be made of the investment and O&M costs of the different subsystems, the daily demands of the desalination plants, the specific energy consumption and the costs of using the grid. In this way, results and conclusions comparable to those of our study can be made in any island of the world.

6. Conclusions

The aim of this paper was to present options to make low-carbon footprint large-scale desalination a reality on arid islands with weak electrical grids. For this, the reconfiguration was proposed of on-grid wind energy systems for water desalination in which large- and medium-scale SWRO plants participate, including control strategies and battery energy storage, to avoid the consumption of energy from the conventional network to which they are connected. The case study considered focuses on the island of Gran Canaria, with its exceptional characteristics for wind energy exploitation, a high desalinated water demand, and a stated desire to achieve a decarbonized economy before the target date set by the EU. From the analyses that were conducted the following conclusions can be drawn:

a) In order to ensure the method has a certain degree of robustness in its search for viable configurations, there is a need to consider the interannual and seasonal evolution of wind speed as opposed to the use of models which use only one series of annual wind speed data, as has been the case to date in the scientific literature.
b) If historical wind data series are not available the use is proposed of data from a global climate reanalysis product, such as ERA5, that covers periods of many years of historical data. However, the results obtained suggest that, to the extent that it is possible, direct use of the ERA5 reanalysis data should not be made and that, instead, machine learning techniques should be employed to fit these data to the actual behaviour of the wind in the study area. This fitting is important given that it will influence calculations of the amount of energy generated by the WF that is injected each hour directly in the conventional grid, the electricity tariffs and the sizing of the BESS. In the case study, the proposed RF model, with its three hyperparameters optimized, was able to fit the ERA5-based wind profile, which is not typical of the area, to its actual wind profile with a relatively good goodness-of-fit.
c) In order to minimize the specific cost of the product water with the proposed on-grid system, it is necessary to substantially increase the size of the WF that is required in the case of operating in accordance with the common strategy of covering the annual desalinated water demand but asynchronously. In the case study, it was necessary to increase the number of 12.5 MW wind turbines from 5 to 26 and include a 3.32 GWh capacity BESS to cover an annual desalinated water demand of 88.622 Hm^3/year, using SWRO plants with a daily capacity of 242,800 m^3/d and a SEC of 3.5 kWh/m^3. The surface area that this BESS would require is considerable and estimated at 4.3 Hm^2.
d) The product water energy cost with the proposed system is 2.87€/m^3. This cost is 7.1 times higher than the cost generated by the SWRO plant if powered from the conventional grid. However, with the proposed system it is possible to eliminate 4,398,310 tCO_2-eq over the 20-year lifetime of the system. In this case, each avoided tCO_2-eq has an associated cost of 1156.6 €.
e) Although the operating strategy considered allows a zero-carbon operational footprint, it is estimated that the current non-reducible carbon footprint over the lifetime of the proposed system would be in the order of 1,285,660 tCO2 eq. Of this footprint, 23.37% (30,052,000 tCO2 eq) is from the SWRO plants and the remaining 76.63% is due to inclusion of the WF and the BESS. That is, a 77.4% reduction of the footprint would be possible if this strategy were applied today with current grid restrictions and a complete LCA carried out in in a societal context that continues to be fossil fuel dependent. However, the remaining 22.6% could be eliminated in the future when manufacturing processes of wind turbines, batteries and desalination plants also receive the benefits of carbon neutral societies.
f) If, given the considerable size of the analysed system (1107 packs of 3 MWh each), a 16% reduction in the specific cost of the BESS (297 €/kWh) and a BESS useful lifetime of 20 years (instead of the 10 considered in the study) were feasible, the number of WTs would be reduced by 15.38% (from 26 to 22), but the BESS capacity would increase by 14.16% (from 3.2 to 3.79 GWh). This has an associated product water specific cost reduction from 3.64€/m^3 to 2.92€/m^3, but a non-eliminated carbon footprint of 1,516,197 tCO_2 eq.
g) If the SWRO plants had a SEC of 3 kWh/m^3, a product water specific cost of 2.57€/m^3 could be obtained. However, this cost is still 6 times higher than the cost which is generated in SWRO plants with capacities ranging between 100,000 and 300,000 m^3/day that use conventional energy.

Nomenclature

a.g.l. above ground level

BESSs battery energy storage systems
BOP balance of plant
C_1, C_2, C_4 and C_5 coefficients that can be obtained from the technical specifications provided by the WT manufacturer
C_3 coefficient that can be estimated from the compiled experimental data
C^R_{BESS} replacement costs of the energy storage subsystem
C_{BESS} initial investment costs of the energy storage subsystem
c_p power coefficient
CPS central power station (Fig. 1)
CRF capital recovery factor
CS control subsystem
C_s estimated specific cost of the product water with each configuration (€/m^3)
CS_WF powers required by the WF during standstill as well as in idle mode
CSP powers demanded by the control system
C_{SWRO} costs associated with investments of the water desalination subsystem
C_{WF} costs associated with the investments that need to be made in the electrical energy generation subsystem
DOD maximum admitted depth of discharge
ECMWF European Centre for Medium-Range Weather Forecasts
ERDs energy recovery devices
ESS energy storage system (Fig. 2)
EU European Union
GFM grid-forming converters
H hour
h height
h_r height below the height *h* of the hub of the WT
I discount rate
i each year in algorithms (Figs. A.1, A.2 and A.3)
j time step in algorithms (Figs. A.1, A.2 and A.3)
L lifetime
L_1 the proportion of estimated losses due to the wake effect of the WTs in the WF
L_2 the proportion of estimated losses due to WT unavailability
L_3 the proportion of estimated losses for environmental reasons (formation of ice and dirt on the blades)
L_4 the proportion of estimated losses due to technical reasons (hysteresis, parasitic load and WT rotor misalignment)
L_5 the proportion of estimated losses when transporting the electrical energy from the transformer at the WF to the on-grid production centre
L_6 the proportion of estimated losses when transporting the wind-sourced electrical energy from the on-grid production centre to the SWRO plants
LCA life cycle assessment
LIBs lithium-ion batteries
LL_B on-load losses of battery
LL_WF on-load losses of WF
M month
MAE mean absolute error
max.depth maximum tree depth in RF
$MBAT_y$ maximum battery energy storage requirements
MIY maximum energy storage capacity
ML machine learning
mtry number of features considered at each split in RF
NLL_B no-load losses of battery
NLL_WF no-load losses of WF
ntree number of trees in RF
NWT number of wind turbines
O&M costs costs associated with the operation and maintenance of the system
P1, P2, P3, P4, P5 and P6 6 different hour-based energy and power periods for the electricity tariff
PCS power conversion subsystem
P_m power that is required to cover the freshwater demand with the SWRO plant of *Qm* capacity and specific consumption SEC_i
PPA power purchase agreement
Qm freshwater flowrate capacity of a desalination plant (m^3/day)
R^2 coefficient of determination
RES renewable energy source
RES-desalination system renewable energy sourced desalination system
RF Random Forest
RMSE root-mean-square error
RTE round-trip DC-to-storage-to-DC energy efficiency of the batteries and the electronic power converters.
S rotor swept area
SCOW simplified cost of water
SDAWES Sea Desalination Autonomous Wind Energy System
SEC specific energy consumption
SOC state of charge
SWRO seawater reverse osmosis
tCO2eq tonnes CO_2 equivalent of emissions
TPV total present value of the actual cost of all the subsystems of a given configuration
UPS uninterrupted power system
$V\_100_{i,j}$ wind speed module for a year *i* and hour *j* at 100 m a.g.l
V_t wind speed at hub height *h* in an instant *t*
VT_h estimated short-term target site wind speeds at the hub height *h*
WF wind farm
WPD wind power density
WSR water storage reservoir (Fig. 2)
$WTPO_t$ power produced by a WT in an instant *t*
WT wind turbine
x,y longitude and latitude components of the ERA5
y_1 period in which battery replacement is made
z_0 surface aerodynamic roughness length
$\overline{WTPO_{min}}$, the mean annual power that a WT of the WF would generate in the year with the lowest wind resource in the series of years considered in the study
$\overline{SC}$ represents the rough initial estimate of the self-consumption of the system, which is considered covered by the energy generated by the WTs

Greek letters

$\Theta\_100_{i,j}$ wind direction for a year *i* and hour *j* at 100 m a.g.l
l tip speed ratio
b pitch angle
r_t air density

CRediT authorship contribution statement

Pedro Cabrera: Writing – review & editing, Writing – original draft, Validation, Resources, Methodology, Investigation, Formal analysis, Data curation, Conceptualization. **José A. Carta:** Writing – review & editing, Writing – original draft, Visualization, Validation, Supervision, Methodology, Investigation, Software, Funding acquisition, Formal analysis, Data curation, Conceptualization, Project administration. **Carlos Matos:** Writing – original draft, Resources, Investigation, Formal analysis, Data curation. **Enrique Rosales-Asensio:** Writing – review & editing, Resources, Investigation, Formal analysis, Data curation. **Henrik Lund:** Writing – review & editing, Writing – original draft, Supervision, Investigation, Formal analysis.

Declaration of competing interest

The authors declare that they have no known competing financial interests or personal relationships that could have appeared to influence the work reported in this paper.

Data availability

Data will be made available on request.

Acknowledgements

This research has been co-funded by the ERDF as part of the INTERREG MAC 2014-2020 program [E5DES Project (MAC2/1.1a/309)].

Appendix A. Schematic description of the method followed for the optimal sizing and simulation of large-scale wind-powered SWRO plants

To select the economically optimal system comprising a stand-alone WF, consisting of a particular number of WTs, *NWT*, and a BESS that allows coverage of a particular hourly freshwater demand, the following diagram was applied.

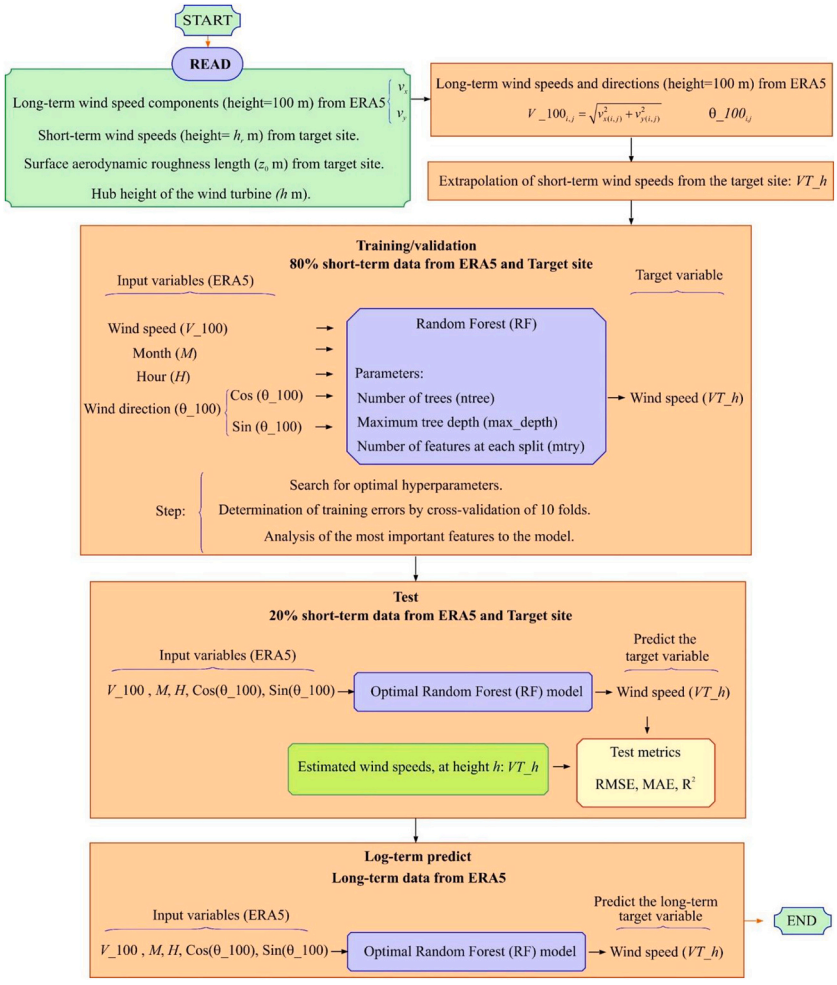

Fig. A.1. Schematic representation of the first task of the method employed.

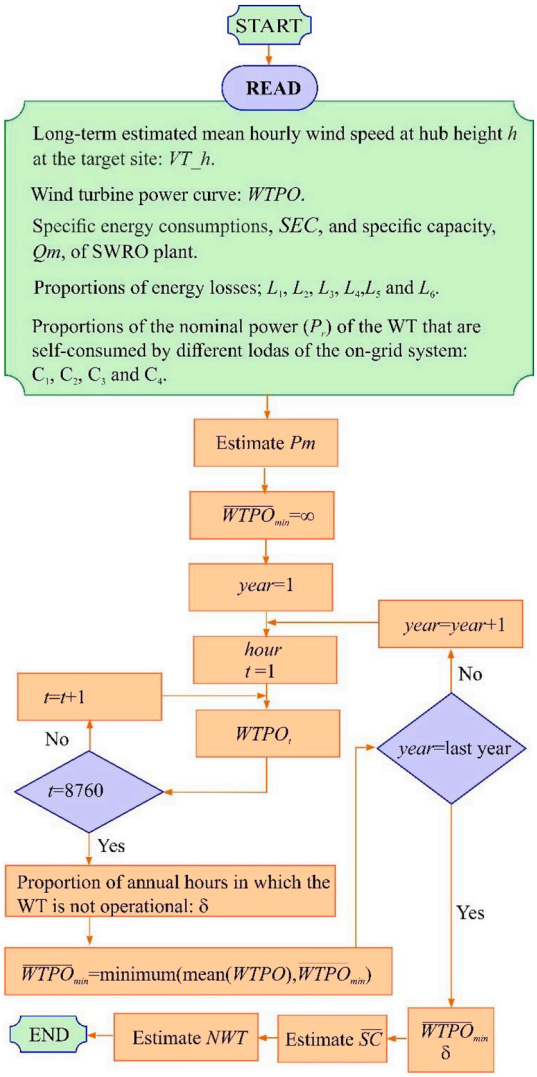

Fig. A.2. Schematic representation of the second task of the method employed.

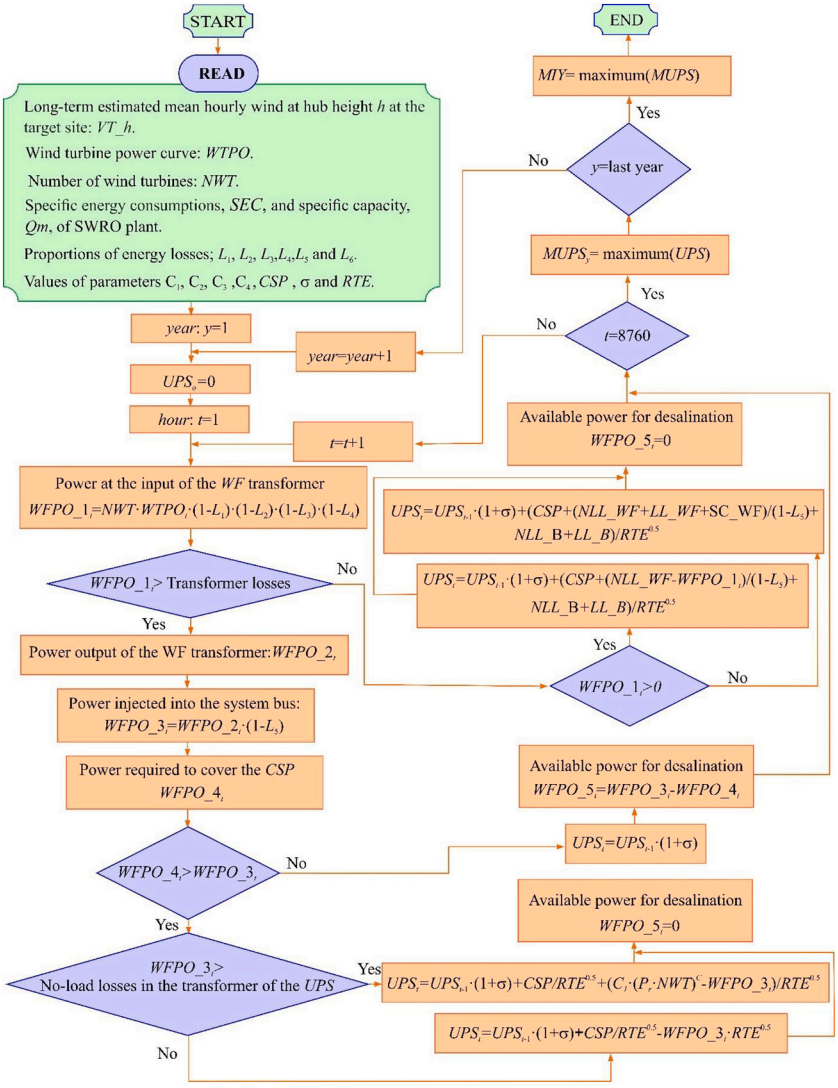

Fig. A.3. Subroutine to estimate the maximum energy storage capacity (*MIY*) in UPS.

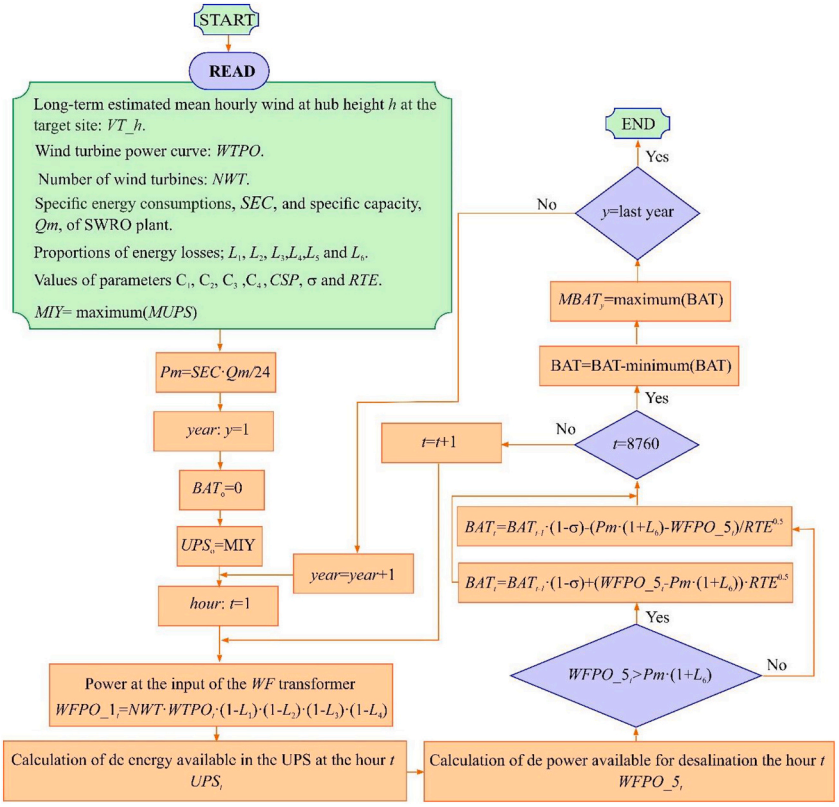

Fig. A.4. Subroutine to estimate the maximum annual capacities ($MBAT_y$) of energy storage in batteries.

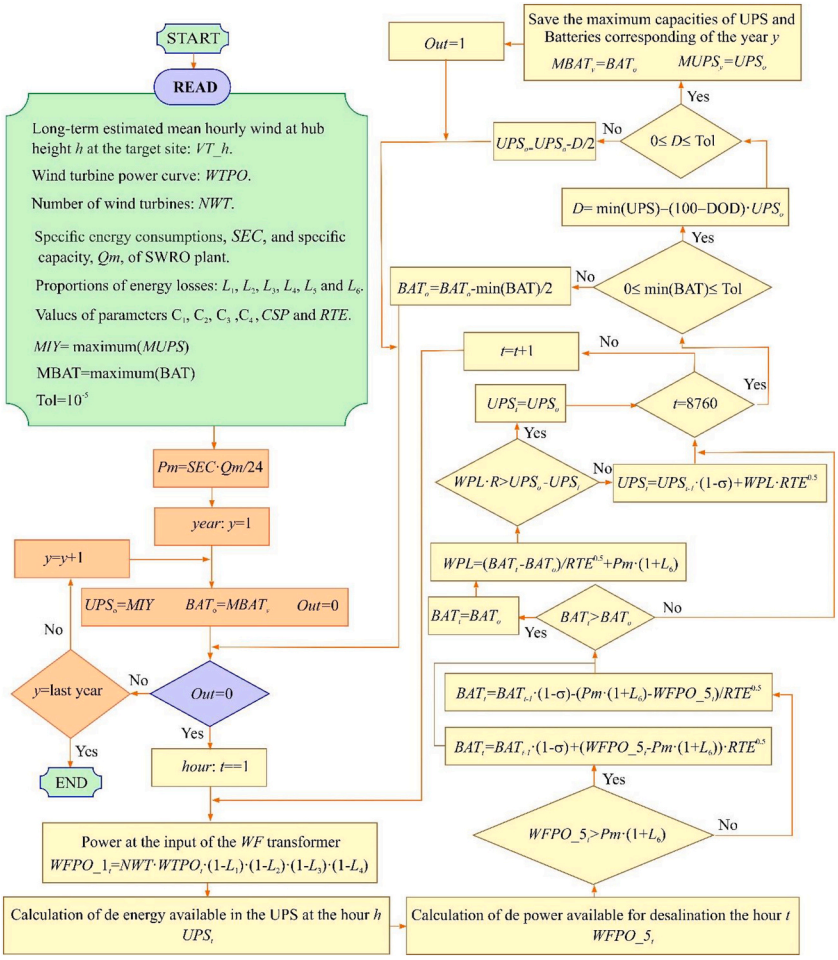

Fig. A.5. Subroutine to delimit the maximum energy storage capacities in UPS and in batteries, BAT.

Appendix B. Data used for the calculation of capital and operating costs for the wind/battery-powered desalination scheme

Table B.1
General equation/input parameter, input parameters and their meaning, and input parameter values used for calculation of capital and operating costs for the wind/battery-powered desalination scheme.

General equation/input parameter	Input parameters meaning	Input parameter value
$C_{WF} = 4200 \times 12{,}500 \times NWT$	C_{WF}: costs associated with the investments that need to be made in the electrical energy generation subsystem *NWT*: number of wind turbines	
$C_{WF}^{O\&M} = 0.03 \times C_{WF}$	$C_{WF}^{O\&M}$: costs associated with the operation and maintenance of the electrical energy generation subsystem C_{WF}: costs associated with the investments that need to be made in the electrical energy generation subsystem	
$C_{SWRO} = 1165 \times 242{,}800$ m^3/d	Costs associated with investments of the water desalination subsystem	
$C_{SWRO}^{O\&M} = 0.106 \times Qm \times 365 + 0.04 \cdot C_{SWRO}$	$C_{SWRO}^{O\&M}$: costs associated with the operation and maintenance of the water desalination subsystem Qm : freshwater flowrate capacity of a desalination plant (m^3/day) C_{SWRO}: costs associated with investments of the water desalination subsystem	
P1, P2, P3, P4, P5 and P6	Hour-based energy and power periods 6 different hour-based energy and power periods for the electricity tariff	
$CRF = \frac{i \cdot (1+i)^L}{(1+i)^L - 1}$	*CRF*: capital recovery factor L: lifetime I: discount rate	*L*: 20 years *i*: 5% of investments at constant prices
L_1, L_2, L_3, L_4, L_5, L_6	Types of energy losses considered and their values L1: the proportion of estimated losses due to the wake effect of the wind turbines in the wind farm L2: the proportion of estimated losses due to wind turbine unavailability L3: the proportion of estimated losses for environmental reasons (formation of ice and dirt	$L_1 = 0.05, L_2 = 0.05, L_3 = 0.005, L_4 = 0.012, L_5 = 0.036$ and $L_6 = 0.047$

(*continued on next page*)

Table B.1 (*continued*)

General equation/input parameter	Input parameters meaning	Input parameter value
	on the blades) L4: the proportion of estimated losses due to technical reasons (hysteresis, parasitic load and wind turbine rotor misalignment) L5: the proportion of estimated losses when transporting the electrical energy from the transformer at the wind farm to the on-grid production centre L6: the proportion of estimated losses when transporting the wind-sourced electrical energy from the on-grid production centre to the seawater reverse osmosis plants	
C_1, C_2, C_3, C_4, C_5, and CSP	Parameters used to estimate the system's energy self-consumption C_1, C_2, C_4 and C_5: coefficients that can be obtained from the technical specifications provided by the wind turbine manufacturer C_3: coefficient that can be estimated from the compiled experimental data CSP: powers demanded by the control system	$C_1 = 0.0132$, $C_2 = 0.7354$, $C_3 = 0.03$, $C_4 = 0.0292$, $C_5 = 0.8043$ and $CSP = 5$ kW
C_{BESS}	Initial investment costs of the energy storage subsystem C_{BESS} includes the cost of the power conversion subsystem, balance of plant and construction and commissioning	297 €/kWh
	Battery useful life before replacement	10 years
$C_{BESS}^{O\&M}$	Costs associated with the O&M of the energy storage subsystem	$C_{BESS}^{O\&M}$ was estimated considering a fixed cost of 6.6 €/kW and a variable cost of 0.025 cent€/kWh
RTE	Round-trip DC-to-storage-to-DC energy efficiency of the batteries and the electronic power converters.	An RTE of 86% was assumed as well as equal charging and discharging efficiency
DOD	Maximum admitted depth of discharge	80%
SOC	State of charge	20%

Appendix C. Results of importance of the predictors in the RF model that was used in the applied procedure

Fig. C.1 shows the variables used as RF model inputs which contributed to reducing the forecasting error of the variable wind speed at the target site at 140 m a.g.l.. Of these variables, the ERA5-based wind speed at 100 m height a.g.l. (V_100) showed the greatest importance. The other variables are trigonometric sin and cos and hour (H) and month (M) of the year.

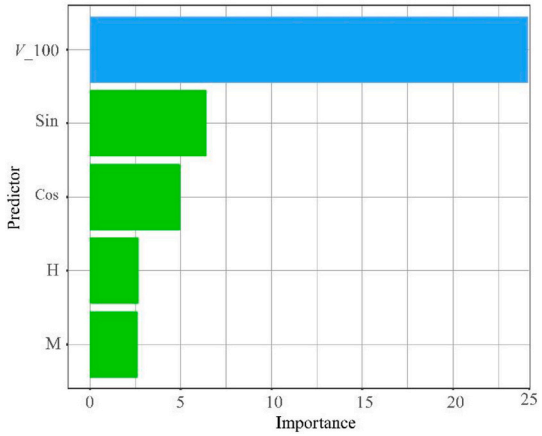

Fig. C.1. Importance of the predictors in the RF model that was used.

Appendix D. Supplementary data

Supplementary data to this article can be found online at https://doi.org/10.1016/j.apenergy.2023.122564.

References

[1] T. United, N. World, W. Development, Water And. 2023.
[2] World Water Assessment Programme (Nations Unies). World water development report 2018 | UN-water, United Nations Educ. Sci Cult Organ New York, United States. https://www.unwater.org/publications/world-water-development-report-2018/; 2018.
[3] Eke J, Yusuf A, Giwa A, Sodiq A. The global status of desalination: an assessment of current desalination technologies, plants and capacity. Desalination. 2020;495:114633. https://doi.org/10.1016/j.desal.2020.114633.
[4] Chen F, Duic N, Manuel Alves L, da Graça Carvalho M. Renewislands-renewable energy solutions for islands. Renew Sustain Energy Rev 2007;11:1888–902. https://doi.org/10.1016/J.RSER.2005.12.009.
[5] Gómez-Gotor A, Del Río-Gamero B, Prieto Prado I, Casañas A. The history of desalination in the Canary Islands. Desalination. 2018;428:86–107. https://doi.org/10.1016/j.desal.2017.10.051.
[6] Jones E, Qadir M, van Vliet MTH, Smakhtin V, Kang S Mu. The state of desalination and brine production: a global outlook. Sci Total Environ 2019;657:1343–56. https://doi.org/10.1016/j.scitotenv.2018.12.076.
[7] Water Desalination. History, advances, and challenges - Manish Kumar, Tyler Culp, and Yuexiao Shen | Frontiers of engineering: Reports on leading-edge engineering from the 2016 symposium |the National Academies Press. https://nap.nationalacademies.org/read/23659/chapter/14; 2023.
[8] Kucera J. Introduction to Desalination. Desalination. 2019:1–49. https://doi.org/10.1002/9781119407874.CH1.
[9] González J, Cabrera P, Carta JA. Wind energy powered Desalination systems. Desalination, Wiley; 2019. p. 567–646. https://doi.org/10.1002/9781119407874.ch14.

[10] Global Clean Water Desalination Alliance. Global Clean Water Desalination Alliance - "H2O minus CO2,". 2015. p. 1–25. http://www.diplomatie.gouv.fr/fr/IMG/pdf/global_water_desalination_alliance_1dec2015_cle8d61cb.pdf.

[11] MIT, GCWDA. Low carbon Desalination status and research, development, and demonstration needs, rep. A work. In: Conduct Massachusetts Inst Technol Assoc With Glob Clean Water Desalin Alliance; 2016. http://web.mit.edu/lowcdesal/.

[12] Aboelmaaref MM, Zayed ME, Zhao J, Li W, Askalany AA, Salem Ahmed M, et al. Hybrid solar desalination systems driven by parabolic trough and parabolic dish CSP technologies: technology categorization, thermodynamic performance and economical assessment. Energ Conver Manage 2020;220:113103. https://doi.org/10.1016/j.enconman.2020.113103.

[13] Mujtaba IM, Sowgath MT. Use of renewable energies in desalination processes. Desalin Technol 2022:515–39. https://doi.org/10.1016/B978-0-12-813790-1.00005-0.

[14] Ghaffour N, Mujtaba IM. Desalination using renewable energy. Desalination. 2018; 435:1–2. https://doi.org/10.1016/j.desal.2018.01.029.

[15] Cherif H, Belhadj J. Environmental life cycle analysis of water desalination processes. Sustain Desalin Handb Plant Sel Des Implement 2018:527–59. https://doi.org/10.1016/B978-0-12-809240-8.00015-0.

[16] Ghaffour N, Lattemann S, Missimer T, Ng KC, Sinha S, Amy G. Renewable energy-driven innovative energy-efficient desalination technologies. Appl Energy 2014; 136:1155–65. https://doi.org/10.1016/j.apenergy.2014.03.033.

[17] Karimanzira D. How to use wind power efficiently for seawater reverse osmosis desalination. Energy Power Eng 2020;12:499–520. https://doi.org/10.4236/epe.2020.129031.

[18] Alawad SM, Ben Mansour R, Al-Sulaiman FA, Rehman S. Renewable energy systems for water desalination applications: a comprehensive review. Energ Conver Manage 2023;286:117035. https://doi.org/10.1016/J.ENCONMAN.2023.117035.

[19] Carta JA, Cabrera P, González J. Wind power integration. Compr Renew Energy 2022:644–720. https://doi.org/10.1016/B978-0-12-819727-1.00102-3.

[20] Segurado R, Madeira JFA, Costa M, Duić N, Carvalho MG. Optimization of a wind powered desalination and pumped hydro storage system. Appl Energy 2016;177: 487–99. https://doi.org/10.1016/J.APENERGY.2016.05.125.

[21] Lund H, Østergaard PA, Connolly D, Mathiesen BV. Smart energy and smart energy systems. Energy. 2017;137:556–65. https://doi.org/10.1016/j.energy.2017.05.123.

[22] Lund H, Thellufsen JZ, Østergaard PA, Sorknæs P, Skov IR, Mathiesen BV. EnergyPLAN – advanced analysis of smart energy systems. Smart Energy 2021;1: 100007. https://doi.org/10.1016/J.SEGY.2021.100007.

[23] Cabrera P, Carta JA, Lund H, Thellufsen JZ. Large-scale optimal integration of wind and solar photovoltaic power in water-energy systems on islands. Energ Conver Manage 2021;235:113982. https://doi.org/10.1016/J.ENCONMAN.2021.113982.

[24] Mathiesen BV, Lund H, Connolly D, Wenzel H, Ostergaard PA, Möller B, et al. Smart energy systems for coherent 100% renewable energy and transport solutions. Appl Energy 2015;145:139–54. https://doi.org/10.1016/J.APENERGY.2015.01.075.

[25] Lund H. Renewable energy systems: A smart energy systems approach to the choice and modeling of 100% renewable solutions. 2nd ed. Massachusetts, USA: Academic Press; 2014. http://www.sciencedirect.com/science/book/9780124104235 (accessed July 16, 2017).

[26] Tzen E. Wind and wave energy for reverse osmosis. Green Energy Technol 2009: 213–45. https://doi.org/10.1007/978-3-642-01150-4_9/COVER.

[27] Plantikow U. Wind-powered MVC seawater desalination — operational results. Desalination. 1999;122:291–9. https://doi.org/10.1016/S0011-9164(99)00049-1.

[28] Windpowered Seawater Desalination - WME GmbH - Public. https://www.wmea.eu/english/download/public/; 2023 (accessed August 15, 2022).

[29] Carta JA, González J, Subiela V. Operational analysis of an innovative wind powered reverse osmosis system installed in the Canary Islands. Sol Energy 2003; 75. https://doi.org/10.1016/S0038-092X(03)00247-0.

[30] Carta JA, González J, Subiela V. The SDAWES project: an ambitious R and D prototype for wind-powered desalination. Desalination. 2004;161. https://doi.org/10.1016/S0011-9164(04)90038-0.

[31] Subiela VJ, Carta JA, González J. The SDAWES project: lessons learnt from an innovative project. Desalination. 2004;168:39–47. https://doi.org/10.1016/j.desal.2004.06.167.

[32] Mentis D, Karalis G, Zervos A, Howells M, Taliotis C, Bazilian M, et al. Desalination using renewable energy sources on the arid islands of South Aegean Sea. Energy. 2016;94:262–72. https://doi.org/10.1016/j.energy.2015.11.003.

[33] Carta JA, Cabrera P. Optimal sizing of stand-alone wind-powered seawater reverse osmosis plants without use of massive energy storage. Appl Energy 2021;304. https://doi.org/10.1016/j.apenergy.2021.117888.

[34] Carta JA, González J, Cabrera P, Subiela VJ. Preliminary experimental analysis of a small-scale prototype SWRO desalination plant, designed for continuous adjustment of its energy consumption to the widely varying power generated by a stand-alone wind turbine. Appl Energy 2015;137. https://doi.org/10.1016/j.apenergy.2014.09.093.

[35] Cabrera P, Carta JA, González J, Melián G. Artificial neural networks applied to manage the variable operation of a simple seawater reverse osmosis plant. Desalination. 2017;416. https://doi.org/10.1016/j.desal.2017.04.032.

[36] Göksu O, Saborío-Romano NA Cutululis, Sørensen PE. Black start and island operation capabilities of wind power plants, APA. 2017.

[37] Technical note ABB medium voltage wind turbine converters enable island mode operation. www.abb.com/converters-inverters; 2014 (accessed May 15, 2023).

[38] Pagnani D, Kocewiak Ł, Hjerrild J, Blaabjerg F, Bak CL. Integrating black start capabilities into offshore wind farms by grid-forming batteries. IET Renew Power Gener 2023. https://doi.org/10.1049/rpg2.12667.

[39] Climate Reanalysis | Copernicus. https://climate.copernicus.eu/climate-reanalysis; 2023 (accessed April 28, 2023).

[40] Voutchkov N. Desalination engineering: Planning and design. New York: McGraw Hill Professional; 2023.

[41] Carta JA, Ramírez P, Velázquez S. A review of wind speed probability distributions used in wind energy analysis. Case studies in the Canary Islands. Renew Sustain Energy Rev 2009;13:933–55. https://doi.org/10.1016/j.rser.2008.05.005.

[42] Consumption of Electricity by Wind Turbines [AWEO.org]. https://www.aweo.org/windconsumption.html; 2023 (accessed May 12, 2023).

[43] Energy efficiency assessment of integrated energy system in substation area | IEEE conference publication | IEEE Xplore. https://ieeexplore.ieee.org/document/8582416; 2023.

[44] Barbulescu C, Kilyeni S, Jigoria-Oprea D, Chiosa N. Electric substation ancillary services power consumption analysis. In: Case study: Timisoara 400/220/110 kV substation, in: ICHQP 2010 - 14th Int. Conf. Harmon. Qual. Power; 2010. https://doi.org/10.1109/ICHQP.2010.5625324.

[45] Pagnam D, Kocewiak LH, Hjerrild J, Blaabjerg F, Bak CL. Overview of black start provision by offshore wind farms. In: IECON proc. (industrial Electron. Conf.). IEEE Computer Society; 2020. p. 1892–8. https://doi.org/10.1109/IECON43393.2020.9254743.

[46] Do you know what an energy PPA is? - Iberdrola. https://www.iberdrola.com/about-us/contracts-ppa-energy; 2023 (accessed April 28, 2023).

[47] Breiman L. Random forests. Mach Learn 2001;45:5–32. https://doi.org/10.1023/A:1010933404324.

[48] Yu S, Vautard R. A transfer method to estimate hub-height wind speed from 10 meters wind speed based on machine learning. Renew Sustain Energy Rev 2022; 169:112897. https://doi.org/10.1016/j.rser.2022.112897.

[49] Díaz S, Carta JA, Matías JM. Performance assessment of five MCP models proposed for the estimation of long-term wind turbine power outputs at a target site using three machine learning techniques. Appl Energy 2018;209:455–77. https://doi.org/10.1016/j.apenergy.2017.11.007.

[50] randomForest: Breiman and Cutler's random forests for classification and regression version 4.6–10 from R-Forge. 2023.

[51] R: The R Project for Statistical Computing. 2023.

[52] Michael C. Brower, wind resource assessment: a practical guide to developing a wind project. Wiley; 2012. https://doi.org/10.1002/9781118249864.

[53] Zhang MH. Wind Resource Assessment and Micro-Siting. Singapore: John Wiley & Sons, Singapore Pte. Ltd; 2015. https://doi.org/10.1002/9781118900116.

[54] Saint-Drenan YM, Besseau R, Jansen M, Staffell I, Troccoli A, Dubus L, et al. A parametric model for wind turbine power curves incorporating environmental conditions. Renew Energy 2020;157:754–68. https://doi.org/10.1016/j.renene.2020.04.123.

[55] Díaz S, Carta JA, Matías JM. Comparison of several measure-correlate-predict models using support vector regression techniques to estimate wind power densities. A case study. Energ Conver Manage 2017;140:334–54. https://doi.org/10.1016/j.enconman.2017.02.064.

[56] Ahmad M, Zeeshan M. Validation of weather reanalysis datasets and geospatial and techno-economic viability and potential assessment of concentrated solar power plants. Energ Conver Manage 2022;256:115366. https://doi.org/10.1016/j.enconman.2022.115366.

[57] Liang Y, Wu C, Zhang M, Ji X, Shen Y, He J, et al. Statistical modelling of the joint probability density function of air density and wind speed for wind resource assessment: a case study from China. Energ Conver Manage 2022;268:116054. https://doi.org/10.1016/j.enconman.2022.116054.

[58] Jain P. Wind energy engineering. 2nd ed. McGraw-Hill Education; 2016.

[59] Beiter P, Musial W, Duffy P, Cooperman A, Shields M, Heimiller D, et al. The cost of floating offshore wind energy in California between 2019 and 2032 cost and performance results data. 2023.

[60] Best Practice Manual For Transformers. https://electrical-engineering-portal.com/download-center/books-and-guides/electrical-engineering/best-practice-manual-transformers; 2023 (accessed June 9, 2023).

[61] China Power Transformer Suppliers. Manufacturers, Factory - Cost Price Power Transformer for Sale - SCOTECH. https://www.scotech-electrical.com/transformer/power-transformer/; 2023 (accessed July 2, 2023).

[62] 66KV Class Three Phase Two Winding OLTC Power Transformer. https://daelim-electric.com/product/66kv-class-three-phase-two-winding-oltc-power-transformer/; 2023 (accessed July 2, 2023).

[63] Examples of Wind Power to Learn From | Energy Central. https://energycentral.com/c/ec/examples-wind-power-learn; 2023 (accessed May 14, 2023).

[64] Mokheimer EMA, Sahin AZ, Al-Sharafi A, Ali AI. Modeling and optimization of hybrid wind-solar-powered reverse osmosis water desalination system in Saudi Arabia. 2023. https://doi.org/10.1016/j.enconman.2013.06.002.

[65] Papapetrou M, Cipollina A, La Commare U, Micale G, Zaragoza G, Kosmadakis G. Assessment of methodologies and data used to calculate desalination costs. Desalination. 2017;419:8–19. https://doi.org/10.1016/j.desal.2017.05.038.

[66] van den Boomen M, Schoenmaker R, Wolfert ARM. A life cycle costing approach for discounting in age and interval replacement optimisation models for civil infrastructure assets. Struct Infrastruct Eng 2018;14:1–13. https://doi.org/10.1080/15732479.2017.1329843.

[67] Díaz-González F, Sumper A, Gomis-Bellmunt O. Energy storage in power systems. Wiley; 2016. https://doi.org/10.1002/9781118971291.

[68] Estrategia Canaria de Acción Climática. https://www.gobiernodecanarias.org/cambioclimatico/materias/estrategia-canaria-accion-climatica/; 2023 (accessed June 24, 2023).

[69] E. Agua en Canarias. Informe de Coyuntura Canario. http://www.gobiernodecanarias.org/istac/jaxi-istac/menu.do?uripub=urn:uuid:4c80614c-ee5b-4f77-aab5-564ec7675fe9; 2014 (accessed June 24, 2023).
[70] Arenas Urrea S, Díaz Reyes F, Peñate Suárez B, de la Fuente Bencomo JA. Technical review, evaluation and efficiency of energy recovery devices installed in the Canary Islands desalination plants. Desalination. 2019;450:54–63. https://doi.org/10.1016/j.desal.2018.07.013.
[71] Observatorio de la Energía de Canarias - Anuarios. https://www3.gobiernodecanarias.org/ceic/energia/oecan/actualidad/articulos-de-opinion; 2023 (accessed June 25, 2023).
[72] Velázquez-Medina S, Santana-Sarmiento F. Evaluation method of marine spaces for the planning and exploitation of offshore wind farms in isolated territories. A two-island case study, ocean. Coast Manag 2023;239:106603. https://doi.org/10.1016/j.ocecoaman.2023.106603.
[73] Schallenberg-Rodríguez J, García Montesdeoca N. Spatial planning to estimate the offshore wind energy potential in coastal regions and islands. Practical case: the Canary Islands. Energy. 2018;143:91–103. https://doi.org/10.1016/j.energy.2017.10.084.
[74] Greenalia Avanza En El Desarrollo De Gofio. https://greenalia.es/noticia/greenalia-avanza-en-el-desarrollo-de-gofio-el-primer-parque-eolico-marino-flotante-de-espana-tras-obtener-el-permiso-aeronautico-por-parte-de-aesa/; 2023 (accessed July 1, 2023).
[75] Proyecto Floating Offshore Wind Canarias (FOWCA) Documento Inicial de Proyecto. www.equinor.com; 2023 (accessed July 1, 2023).
[76] de Assis Tavares LF, Shadman M, de Assad LPF, Estefen SF. Influence of the WRF model and atmospheric reanalysis on the offshore wind resource potential and cost estimation: a case study for Rio de Janeiro State. Energy. 2022;240:122767. https://doi.org/10.1016/j.energy.2021.122767.
[77] Las nuevas tarifas para contratos de más de 15 kW o de alta tensión | El Blog de Som Energia. https://blog.somenergia.coop/destacados/2021/04/las-nuevas-tarifas-para-contratos-de-mas-de-15-kw-o-de-alta-tension/#nuevas6; 2023 (accessed July 2, 2023).
[78] Mongird K, Fotedar V, Viswanathan V, Koritarov V, Balducci P, Hadjerioua B, et al. Energy Storage Technology and Cost Characterization Report. 2019.
[79] Notton G. Hybrid wind-photovoltaic energy systems. In: Stand-Alone Hybrid Wind Energy Syst. Elsevier; 2010. p. 216–53. https://doi.org/10.1533/9781845699628.2.216.
[80] Tesla''s massive 1GWh Megapack battery project with PG&E is approved | Electrek. https://electrek.co/2020/02/27/tesla-1gwh-megapack-battery-project-pge-approved/; 2023 (accessed July 17, 2023).
[81] Martinez A, Iglesias G. Mapping of the levelised cost of energy for floating offshore wind in the European Atlantic. Renew Sustain Energy Rev 2022;154:111889. https://doi.org/10.1016/j.rser.2021.111889.
[82] Garcia-Teruel A, Rinaldi G, Thies PR, Johanning L, Jeffrey H. Life cycle assessment of floating offshore wind farms: an evaluation of operation and maintenance. Appl Energy 2022;307:118067. https://doi.org/10.1016/j.apenergy.2021.118067.
[83] Yudhistira R, Khatiwada D, Sanchez F. A comparative life cycle assessment of lithium-ion and lead-acid batteries for grid energy storage. J Clean Prod 2022;358:131999. https://doi.org/10.1016/j.jclepro.2022.131999.
[84] Najjar E, Al-Hindi M, Massoud M, Saad W. Life cycle assessment of a seawater reverse osmosis plant powered by a hybrid energy system (fossil fuel and waste to energy). Energy Rep 2021;7:448–65. https://doi.org/10.1016/j.egyr.2021.07.106.
[85] New: Tesla Unveils Megapack Order Page & Pricing - Tesla Daily. https://www.thestreet.com/tesla/news/new-tesla-megapack-details-price; 2023 (accessed July 17, 2023).
[86] Karagiannis IC, Soldatos PG. Water desalination cost literature: review and assessment. Desalination. 2008;223:448–56. https://doi.org/10.1016/j.desal.2007.02.071.
[87] Wei M, Patadia S, Kammen DM. Putting renewables and energy efficiency to work: how many jobs can the clean energy industry generate in the US? Energy Policy 2021;38(2):919–31.
[88] IEA. Technology roadmap - China wind energy development roadmap 2050, IEA, Paris. https://www.iea.org/reports/technology-roadmap-china-wind-energy-development-roadmap-2050; 2011.
[89] AECOM. Evaluating Benefits of Offshore Wind Energy Projects in NEPA. US Dept. of the Interior, Bureau of Ocean Energy Management, Headquarters, Sterling VA. OCS Study BOEM 2017-048. 2017. p. 94.
[90] Tegen S, Keyser D, Flores-Espino F, Miles J, Zammit D, Loomis D. Offshore wind jobs and economic development impacts in the United States: Four regional scenarios. United States: N. P; 2015. https://doi.org/10.2172/1171787. Web.
[91] IRENA and ILO. Renewable energy and jobs – Annual review 2021. Abu Dhabi, Geneva: International Renewable Energy Agency, International Labour Organization; 2021.
[92] GWEC. Wind power & green recovery. https://gwec.net/wp-content/uploads/2021/04/Jobs-Note-April-2021-2.pdf; 2023 [accessed on 06.11.2023].
[93] Energy Policy Group. Romania's offshore wind energy resources: natural potential, regulatory framework, and development prospects2020; 2020.
[94] Costa H, Veiga L. Local labor impact of wind energy investment: an analysis of Portuguese municipalities. Energy Econ 2021;94:105055.